



HAL
open science

Chiral Smectic C Liquid Crystal, Thick Sample Textures

M. Brunet, Ph. Martinot-Lagarde

► **To cite this version:**

M. Brunet, Ph. Martinot-Lagarde. Chiral Smectic C Liquid Crystal, Thick Sample Textures. Journal de Physique II, 1996, 6 (12), pp.1687-1725. 10.1051/jp2:1996157 . jpa-00248402

HAL Id: jpa-00248402

<https://hal.science/jpa-00248402>

Submitted on 4 Feb 2008

HAL is a multi-disciplinary open access archive for the deposit and dissemination of scientific research documents, whether they are published or not. The documents may come from teaching and research institutions in France or abroad, or from public or private research centers.

L'archive ouverte pluridisciplinaire **HAL**, est destinée au dépôt et à la diffusion de documents scientifiques de niveau recherche, publiés ou non, émanant des établissements d'enseignement et de recherche français ou étrangers, des laboratoires publics ou privés.

Chiral Smectic C Liquid Crystal, Thick Sample Textures

M. Brunet (^{1,*}) and Ph. Martinot-Lagarde (²)

(¹) G.D.P.C. Université Montpellier II, 34095 Montpellier. France

(²) Physique des Solides, Bâtiment 510, Université Paris-Sud, 91405 Orsay, France

(Received 11 December 1995, revised 31 July 1996, accepted 9 September 1996)

PACS.61.30.-v – Liquid crystals

PACS.61.72.Lk – Linear defects: dislocations, disclinations

Abstract. — The texture of ferroelectric chiral smectic liquid crystal confined between two aligning plates is studied in the case of thick samples *i.e.* samples whose thickness is higher than the helical pitch. The helical texture with periodic *unwinding disclination lines* appears in these samples. A theoretical elastic calculation is made assuming in the defect lines the melting of the smectic C phase into the smectic A phase. It allows the calculation of the line positions and the local helical pitch *versus* the sample thickness. In the case of the *bookshelf* geometry and in that of the *chevron* our observations are well explained by the model. The pitch measurement allows an estimation of the defect core energy and confirms the A melting. We show the existence of the chevron plane in thick samples, plane which plays the role of an unwinding surface, for the helical structure.

Résumé. — Nous étudions la texture du cristal liquide smectique C chiral ferroélectrique, confiné entre deux lames de verre traitées, dans le cas d'un échantillon épais, c'est-à-dire tel que l'épaisseur soit supérieure au pas de l'hélice. On observe une texture enroulée accompagnée de lignes de disinclinaison dites *lignes de déroulement*. Nous présentons un calcul du minimum de l'énergie élastique en supposant, dans les lignes de défaut, une fusion de la phase smectique C dans la phase smectique A. Cette hypothèse permet de calculer la position des lignes et le pas hélicoïdal local en fonction de l'épaisseur de l'échantillon. Nos résultats expérimentaux sont bien expliqués par le modèle dans le cas de la géométrie dite en *bookshelf* et dans le cas du *chevron*. La mesure du pas permet d'évaluer l'énergie du cœur du défaut et confirme la fusion en phase A. Nous montrons l'existence du plan du chevron dans les échantillons épais, plan qui joue pour la structure hélicoïdale le rôle de surface de déroulement.

Introduction

The chiral smectic C phase [1] (C* phase) is made of layers. In the layers the molecules are tilted with an angle θ_0 with respect to the layer normal. The layers pile up while turning with a spontaneous pitch Z_0 , it is a liquid (2D) in the layers, a solid (1D) in the direction perpendicular to the layers. It possesses only a helical symmetry and a twofold axis. This lack of symmetry allows a spontaneous electrical polarization \mathbf{P} . It also gives rise to difficult adjustment between the spontaneous helical texture and the homogeneous texture often imposed by sample walls.

(*) Author for correspondence (e-mail: brunet@gdpc.univ-mont2.fr)

This phase has been studied in detail for thin samples because of the possible applications as displays. In this case the texture is more connected with the surface interactions than with the bulk properties.

In this paper we study the texture of thick samples. We give an elastic model of the defect lines that appear between the helical sample bulk and the homogeneous sample part near the walls. This model allows us to calculate the appearance and the position of these lines. We compare these predictions with the sample observations.

1. The Thick Sample Textures

In thick samples, prepared with untreated glass plates, it is well-known that the texture of a chiral smectic C shows more or less regular arrays of lines (Photo 1, p. 1713), first called stripes, and focal conics. They have been interpreted as the result of the connection between the helical structure in the bulk and the unwound structure imposed by the bounding surfaces. First called "dechiralization lines" we now prefer unwinding lines because, on the surfaces, the structure is unwound and not dechiralized.

These lines are located close to the surfaces but in the bulk. They go in pairs, one line of the pair is located close to one surface, the other line close to the other surface. The relative positions of the two lines of a pair change in relation to the relative anchoring direction on the two surfaces. The two lines of a pair can be superposed when the anchoring directions are parallel. Figure 1 shows these superposed lines with extinction of the background between crossed polarizers, indicating parallel anchoring. The observations were made on a mixture with no smectic A phase, and having a very small spontaneous polarization. A strong planar anchoring is obtained by SiO evaporation at 60° incidence.

The lines can also be shifted forward a half pitch. Figure 2 shows these shifted lines with extinction of the background. The angle between polarizers is 50° that is about $\pi/2 - 2\theta_0$, which indicates symmetrical anchoring. The direction of the polarizer, of the analyzer, of the aligning direction and the anchoring directions on both the glass plates deduced from the extinction are indicated in Figure 2. The observations were made in a pure chiral smectic C compound presenting a smectic A phase and having a medium spontaneous polarization; the surface treatment is the same as in Figure 1.

The first situation is similar to a uniform molecular orientation parallel to the plates in Surface Stabilized Ferroelectric Liquid Crystal (SSFLC) [2] geometry (thin samples), the electrical polarization lying along the normal to the plates. The second one is similar to a rotation of a half turn on the cone for the molecules going from the lower to the upper surface. This situation is often called a splayed structure [3]. The interpretation was made assuming the smectic layers perpendicular to the glass plates, a structure called "bookshelf" geometry. The topology of the director field for superposed lines described by Brunet et Williams [4] is recalled in Figure 3a and that for shifted lines described by Glogarova and Pavel [5] recalled in Figure 3b.

Sometimes we observe lines on the plates as shown in Figure 21 the corresponding texture is drawn in Figure 22. They are separated on the surface by half a pitch. This configuration indicates a bistable surface anchoring [6], a quasi degenerated planar anchoring or some surface hysteresis.

Most of the studies during the last years were made for compounds with the $N^* - S_A$ transition and under experimental conditions (surface treatment, spontaneous polarization, *etc.*) giving rise to a symmetrical anchoring where the thickness exceeds about $1.5 \mu\text{m}$. We can invoke two effects to explain the frequent occurrence of the symmetrical anchoring. The spontaneous polarization interaction with the surface polarization gives a polar surface energy term. Also

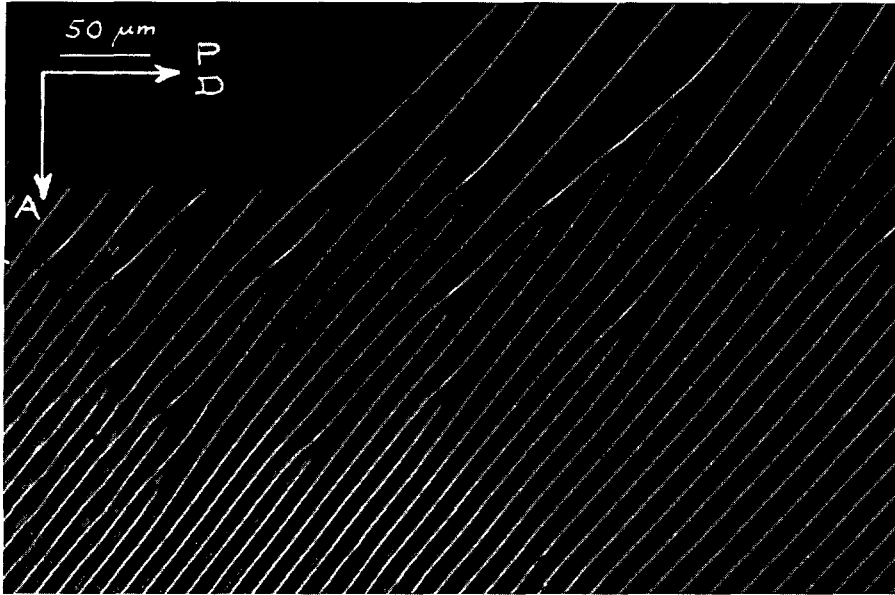


Fig. 1. — Regular array of pairs of superposed lines. The extinction of the background between crossed polarizers (A and P) shows that the anchoring directions on both surfaces are parallel to the aligning direction (D). The distance between two neighbouring lines is about $15 \mu\text{m}$. Compound: a 5% mixture of cholesteryl cinnamate with bis-(4'-n-decyloxybenzal) 2-chloro-1-4-phenylenediamine. The cell geometry is cylindrical: a cylindrical lens ($R = 102 \text{ mm}$) is put on a glass plate. The thickness is growing from the top to the bottom of the photo.

the molecular chirality creates a spontaneous bend. This spontaneous bend does not appear in the bulk elastic energy because it can be integrated, but this integration gives a polar surface term [7].

2. Calculations of Limited Sample Textures

2.1. HYPOTHESIS AND EQUATIONS. — To obtain the texture of a limited sample we define the geometrical conditions and the defect model; we then calculate the involved elastic energies, and minimize these energies by solving numerically the Euler equations.

2.1.1. *Geometrical Conditions.* — To simplify our study we use the following model:

- On the surfaces the molecules lie parallel to the plates, the anchoring is very strong. The distance between the plates is d .
- The smectic layers in equilibrium are normal to the plates. The z axis is their normal. (Fig. 4a). θ is the tilt angle of the molecular director with respect to z , the local normal to the layer. φ is the azimuth angle with respect to x , the normal to the plate.
- The texture has only two dimensions and does not vary along the y direction, parallel to the plates and to the smectic layers.
- The x axis is the normal to the plates perpendicular to y and z .

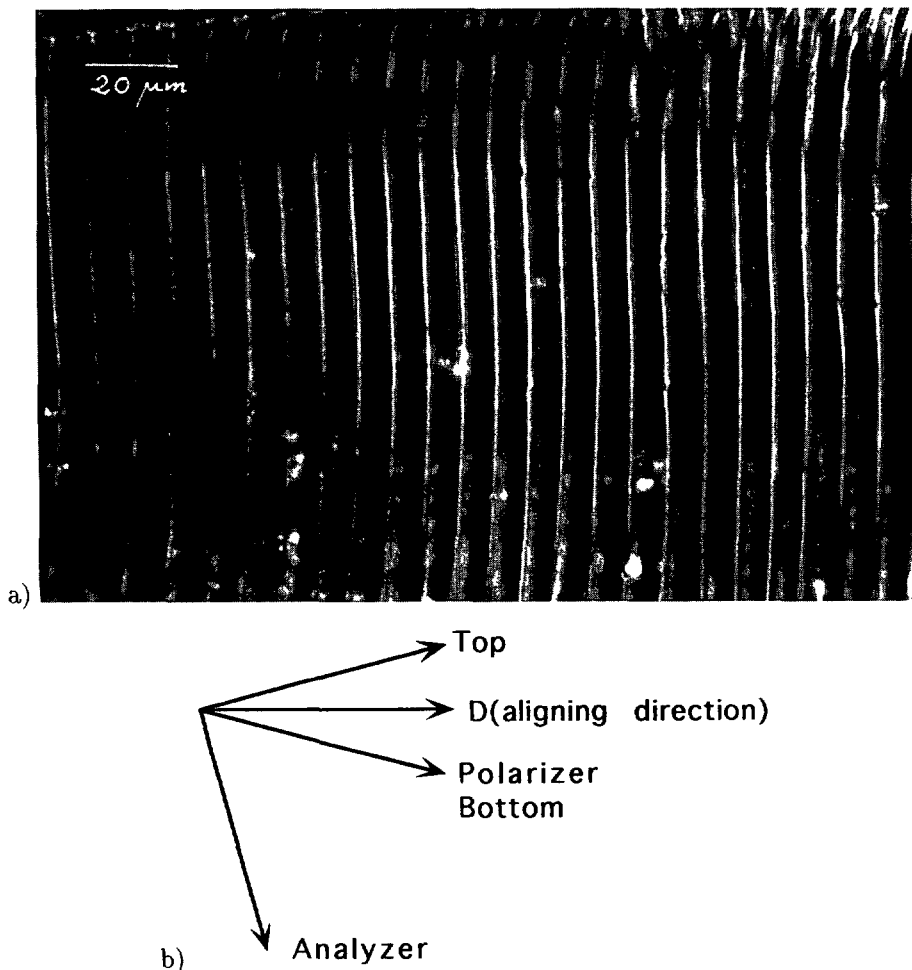


Fig. 2. — Regular array of pairs of shifted lines. The polarizer (P) and the analyzer (A) make an angle of 50° (that is about $\pi/2 - 2\theta$), when is obtained the extinction of the background; it shows that the anchoring directions on both surfaces (Bottom: B and Top: T) are symmetrical with respect to the layer normal which is parallel to the aligning direction (D). The distance between two neighbouring lines is about $10 \mu\text{m}$. Compound: a 50% mixture of chiral p-decyloxybenzylidene p'-amino 2-methyl butyl cinnamate (D.O.B.A.M.B.C.) with the racemic. Cell thickness: about $30 \mu\text{m}$.

- The layer deformation is defined by u its displacement along z with respect to its equilibrium position.
- The molecular orientation is defined in the layer with respect to a local frame: $x_1 y z_1$, as shown in Figure 4b. θ is the tilt angle of the molecular director with respect to z_1 the local normal to the layer. φ is the azimuth angle with respect to x_1 , in the layer and perpendicular to y .

2.1.2. *Defect Line Model.* — In the defect line, topological argument indicates a φ jump of π if θ is kept constant. To obtain a continuous variation of the molecular orientation, we imagine

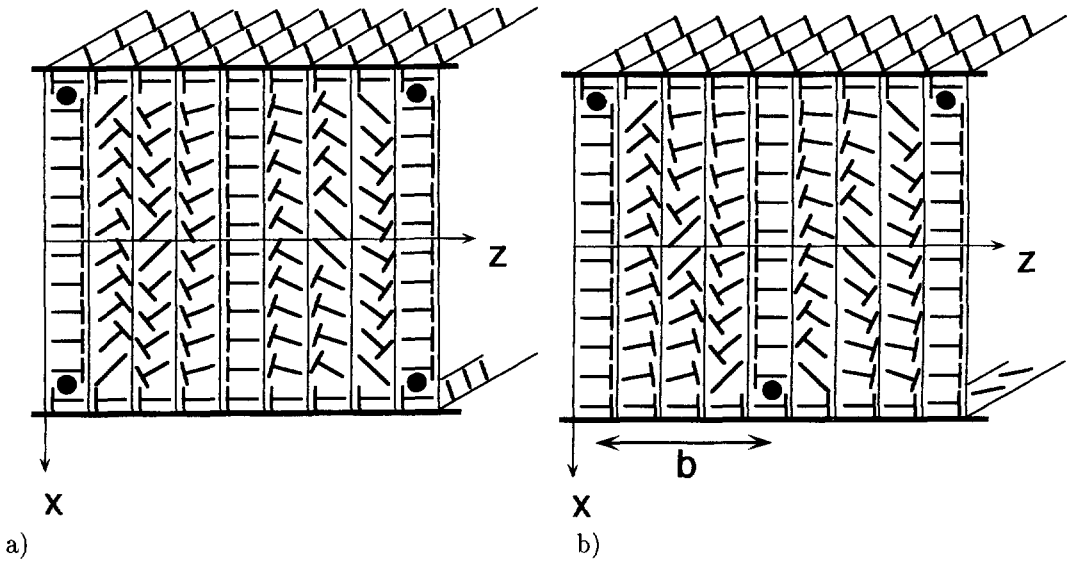


Fig. 3. — Topology of the director in two cases of planar molecular anchoring on the surfaces: a) parallel anchoring, b) symmetrical anchoring. The distance b between the two families of defects lines is 0 in 3a and $Z_0/2$ in 3b.

a core of the defect where the molecules are normal to the smectic layer ($\theta = 0$, φ undefined). The π jump of φ is then transformed in a continuous variation of θ from $-\theta_0$ to $+\theta_0$ without φ discontinuity. This corresponds to a second order transition from the C* phase in the bulk to the A phase in the defect core. Figure 5 shows a drawing of the defect. The A melting corresponds to an increase of the layer thickness. This induces a displacement u of the layers. This displacement propagates along the normal to the layer near the plane parallel to the plates and going through the defect, because a smectic layer is like a sheet of paper it is easy to bend and difficult to compress [8].

2.1.3. *Involved Energies.* — The infinite sample equilibrium texture is made of constant thickness parallel plane layers. In the layer the molecules are parallel and tilted with θ_0 . They turn from one layer to the other making a helix of pitch Z_0 .

In the central part of a sufficiently thick sample the helical equilibrium is reached. The uniform boundary conditions imposed by the plates create a distortion, the corresponding energy density can be separated into nematic energy, smectic tilt energy and smectic compression energy:

$$F = F_n + F_{S\theta} + F_{SC}$$

We call nematic energy the energy corresponding to a variation of the director direction [9]. It is function of the derivative of φ and θ and of the second derivative of u . The derivatives of φ and θ measure the molecular orientation variation in the layer. The second derivative of u , measures the molecular orientation variation due to the layer bending. For low displacement of the layer, in the approximation of only one elastic constant K and if we neglect fourth order energy terms in θ , we write the nematic energy density F_n as:

$$F_n = \frac{K}{2} \left\{ \theta^2 \left(\frac{\partial \varphi}{\partial x} \right)^2 + \theta^2 \left(\frac{\partial \varphi}{\partial z} - \frac{2\pi}{Z_0} \right)^2 + \left(\frac{\partial \theta}{\partial x} \right)^2 + \left(\frac{\partial \theta}{\partial z} \right)^2 + \left(\frac{\partial^2 u}{\partial x^2} \right)^2 - \frac{2\partial^2 u}{\partial x^2} \frac{\partial(\theta \cos \varphi)}{\partial x} \right\}$$

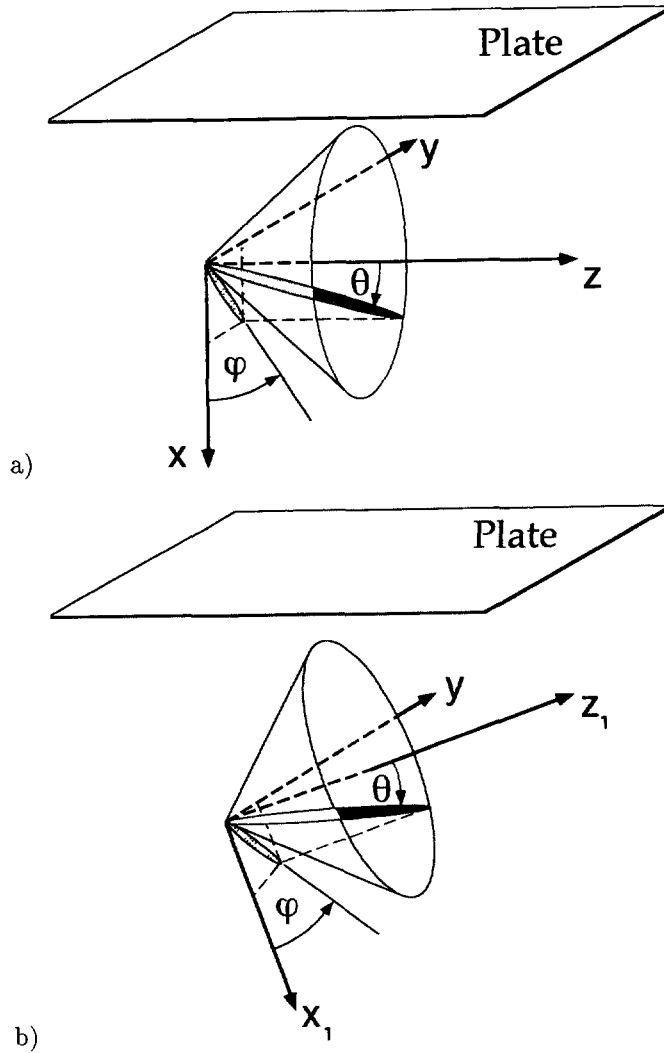


Fig. 4. — a) In equilibrium the smectic layers are normal to the plates. The angles which define the molecular orientation in the layer are the tilt angle θ , with respect to the layer normal \mathbf{z} , the azimuthal angle φ , with respect to the normal to the plates, \mathbf{x} . b) The molecular orientation is defined in the layer with respect to a local frame, $\mathbf{x}_1, \mathbf{y}_1, \mathbf{z}_1$: the tilt angle θ , in relation with the local normal to the layer, \mathbf{z}_1 , the azimuthal angle φ , in relation with \mathbf{x}_1 , in the layer and perpendicular to \mathbf{y} .

The smectic tilt energy density $F_{S\theta}$ corresponds to the torque that keeps the molecules at the equilibrium tilt θ_0 [10]:

$$F_{S\theta} = \frac{K}{4\mu^2} (\theta^2 - \theta_0^2)^2$$

The length μ gives the ratio between the nematic constant K and the smectic tilt constant. This energy appears in the defect line when θ goes to 0.

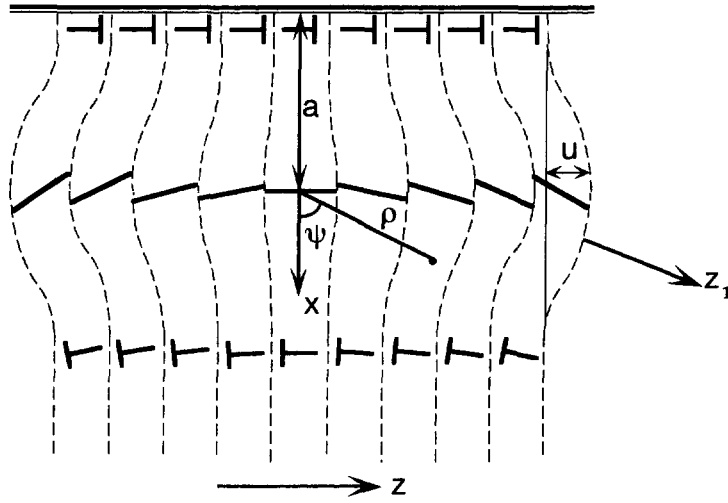


Fig. 5. — A model of the unwinding line defect. The u displacement propagates along the layer normal z . The axis z_1 is defined in Figure 4b. (ρ, ψ) are cylindrical coordinates around the defect. In the core the molecules are normal to the layer. They melt in smectic A phase.

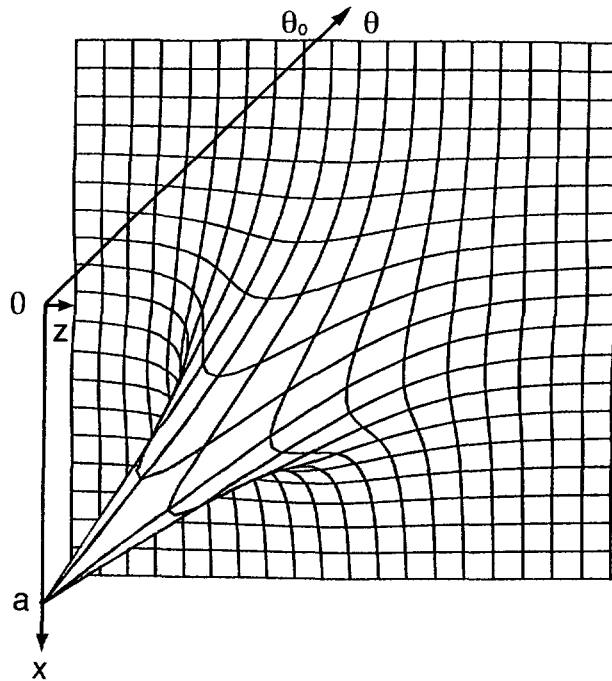


Fig. 6. — The molecular tilt angle θ near a line versus z and the distance from one plate x . On the plate ($x = 0$) the equilibrium angle $\theta_0 = 0.1$ radian is obtained. The tilt angle is zero in the defect core ($x = a, z = 0$).

The smectic compression energy density F_{SC} is [11, 12]:

$$F_{SC} = \frac{K}{2\lambda^2} \left(\frac{\partial u}{\partial z} + \frac{(\theta^2 - \theta_0^2)}{2} \right)^2$$

The length λ gives the ratio between the nematic elastic constant and the compression energy constant. This energy appears near the defect line because of the layer thickness increase in the defect line due to the melting in smectic A. We neglect the layer shear energy in $(\partial u / \partial x)^2$ because of its second order in u . Nevertheless, in $F_{S\theta}$ and F_{SC} , we keep fourth order terms in θ because the lengths λ and μ are so small that the coefficient of this kind of energy is very important.

We do not take into account the electrical energy because we are interested in the texture of samples without any applied field. The only electrical effect is due to the divergence of \mathbf{P} , the spontaneous polarization. The corresponding charges are in the defect line. They are screened by the ionic impurities. In very pure and chemically stable compounds, charges remain but it is possible to demonstrate that the corresponding effect only renormalize the nematic constant in the simple case of one nematic elastic constant we are using.

2.1.4. Euler Equations. — The equilibrium configuration minimizes these energies. It is the solution of the Euler equations obtained by functional derivation of the previous energy densities:

$$\begin{aligned} \theta \left(\frac{\partial^2 \varphi}{\partial x^2} + \frac{\partial^2 \varphi}{\partial z^2} \right) + 2 \frac{\partial \theta}{\partial x} \frac{\partial \varphi}{\partial x} + 2 \frac{\partial \theta}{\partial z} \left(\frac{\partial \varphi}{\partial z} - \frac{2\pi}{Z_0} \right) + \sin \varphi \frac{\partial^3 u}{\partial x^3} &= 0 \\ - \left(\frac{\partial^2 \theta}{\partial x^2} + \frac{\partial^2 \theta}{\partial z^2} \right) + \theta \left[\left(\frac{\partial \varphi}{\partial x} \right)^2 + \left(\frac{\partial \varphi}{\partial z} - \frac{2\pi}{Z_0} \right)^2 \right] & \\ + \left(\frac{1}{\mu^2} + \frac{1}{2\lambda^2} \right) \theta (\theta^2 - \theta_0^2) + \frac{\theta}{\lambda^2} \frac{\partial u}{\partial z} + \cos \varphi \frac{\partial^3 u}{\partial x^3} &= 0 \\ - \frac{\partial^4 u}{\partial x^4} + \frac{1}{\lambda^2} \left(\frac{\partial^2 u}{\partial z^2} + \theta \frac{\partial \theta}{\partial z} \right) + \frac{\partial^3}{\partial x^3} (\theta \cos \varphi) &= 0 \end{aligned}$$

Because of the non linearity of this system we only compute a numerical solution by a relaxation method [13]. In this calculation θ is kept positive and φ varies from $-\pi/2$ to $3\pi/2$. these conventions do not change the continuous model indicated in paragraph 2.1.2.

2.2. RESULTS OF THE NUMERICAL CALCULATION AND COMPARISON WITH ANALYTIC APPROXIMATIONS. — The calculations are made for $Z_0 = Z = d = 2 \mu\text{m}$ when, as we will see later, the helical structure may exist in some cases but is very constrained by the proximity of the plates. The values $\mu = 30 \text{ \AA}$, $\lambda = 20 \text{ \AA}$ are an order of magnitude obtained from the measures of Galerne [9] near the smectic A \rightarrow C transition (100 \AA and 50 \AA) by dividing by 3 these values to take into account the saturation of the constants far from the transition. The positions of the defect lines are fixed. They are superimposed or shifted of half a pitch depending of the anchoring. The distance a between the defect line and the neighbouring plate is fixed as: $a = Z_0/4\pi$. These positions will be examined in paragraph 2.3.

2.2.1. The Tilt Angle θ Variations. — In Figure 6 are drawn the values of the tilt angle θ versus z and x for $\theta_0 = 0.1$ radian, in the case of parallel anchoring on the two surfaces ($\varphi_1 = \varphi_2 = \pi/2$).

We can observe in this drawing that θ varies only in a cylinder of radius r , the core of the defect. Outside of this cylinder, θ is very close to θ_0 . The comparison between $\theta(a, z)$ and

$\theta(x,0)$ shows the cylindrical symmetry of the defect even in this case of $Z_0 = d$ where the interaction with the plates may brake the cylindrical symmetry. The calculation made for the symmetrical anchoring ($\varphi_1 = -\varphi_2 = \pi/2$) and for the surface line case ($\varphi_1 = \varphi_2 = \pm\pi/2$) gives the same result. However, in the last case, the defect is cut along its axis by the sample plate (Fig. 22).

An approximate simple expression of the θ variation in the defect core can be obtained if we take into account the cylindrical symmetry of the computer result. The energy can be written in cylindrical coordinates (ρ, ψ) around the defect (Fig. 5) as:

$$\frac{K}{2} \int_0^\infty \left[\frac{(\theta^2 - \theta_0^2)^2}{2\mu^2} + \frac{\theta^2}{\rho^2} + \left(\frac{\partial\theta}{\partial\rho} \right)^2 \right] 2\pi\rho d\rho$$

In this expression we neglect the compression energy because we postulate the defect core as incompressible and the spontaneous pitch is supposed large enough to be neglected in the defect core. The nematic energy is very simple because the cylindrical symmetry gives $\partial\varphi/\partial\rho = 0$, $\partial\varphi/\partial\psi = 1$ and $\partial\theta/\partial\psi = 0$. The corresponding Euler equation for θ is:

$$\rho \frac{\theta(\theta^2 - \theta_0^2)}{\mu^2} + \frac{\theta}{\rho} - \frac{\partial\theta}{\partial\rho} - \rho \frac{\partial^2\theta}{\partial\rho^2} = 0$$

For low ρ this equation reduces to $\frac{\theta}{\rho} = \frac{\partial\theta}{\partial\rho}$ and gives θ proportional to ρ .

For large ρ , the equation is:

$$\frac{\theta}{\theta_0} \left(\frac{\theta^2}{\theta_0^2} - 1 \right) = \frac{\mu^2}{\theta_0^2} \frac{\partial^2}{\partial\rho^2} \left(\frac{\theta}{\theta_0} \right)$$

and it has the solution:

$$\theta = \theta_0 \tanh \frac{\rho}{r'} \quad \text{with} \quad r' = \frac{\sqrt{2}}{\theta_0} \mu$$

The defect core radius r given by the numerical calculation is plotted in Figure 7 *versus* θ_0 . r is defined by the derivative of θ *versus* ρ near the defect center:

$$\frac{\theta_0}{r} = \frac{\partial\theta}{\partial\rho} \text{ if } \rho \rightarrow 0$$

The concordance with the analytical approximation r' is good.

The calculation indicates that the θ distortion is only located in a very small volume of the sample near the defect lines. This volume increases only near the A \rightarrow C* transition where θ_0 tends to zero.

2.2.2. Smectic Layer Displacement Variation. — In Figure 8 is drawn the layer displacement u *versus* x and z for $\theta_0 = 0.4$ radian and the parallel anchoring ($\varphi_1 = \varphi_2 = \pi/2$). This displacement is created by the layer thickness increase in the defect core due to the θ decrease. We can see as expected that this distortion only stays in a domain parallel to the plates of thickness close to twice the core radius. In this domain the maximum displacement is reached at a distance from the defect center larger than the defect core radius ($z \approx 2r$). The calculation gives a linear decrease of u *versus* z for $z > 2r$, it corresponds to a uniform compression of the sample in this region.

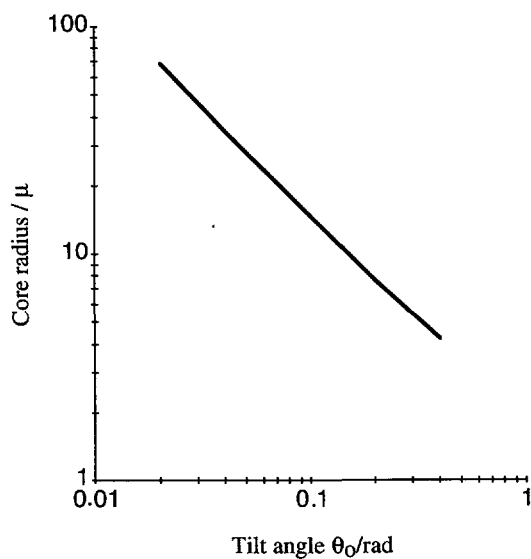


Fig. 7. — log-log plot of the line core radius r versus the tilt angle θ . r is divided by μ , the characteristic length of the smectic C energy. The calculation is made for $Z_0 = d = 2 \mu\text{m}$, $\mu = 30 \mu\text{m}$ and $\lambda = 20 \mu\text{m}$. One can see that r is inversely proportional to θ_0 .

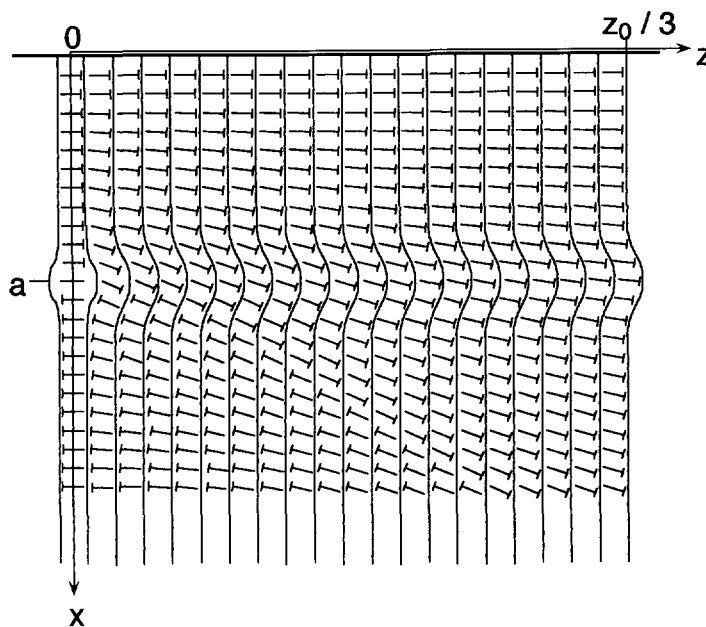


Fig. 8. — Sketch of the layer displacement u versus z and x , for $\theta_0 = 0.4$ radian. The layer thickness increase in the defect core induces a layer displacement u which propagates in the direction normal to the layer until the half pitch of the texture.

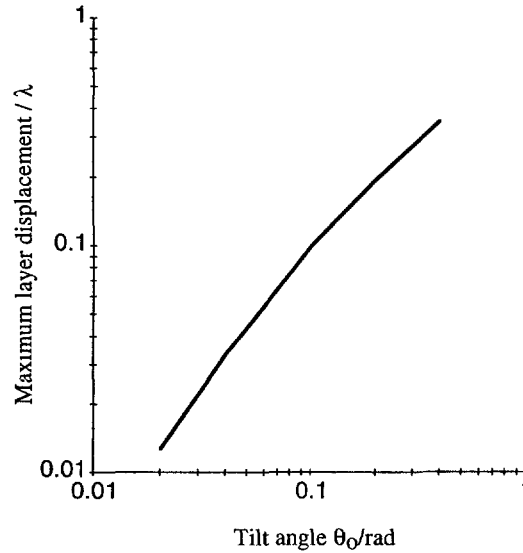


Fig. 9. — log-log plot of the maximum layer displacement *versus* the equilibrium tilt angle θ_0 . The displacement is reported to λ , the characteristic length of the smectic compression energy. The parameters are the same as in Figure 7.

In Figure 9 is plotted the maximum of the displacement *versus* the equilibrium tilt angle θ_0 . Around $\theta_0 = 0.1$ radian a linear variation of u_{\max} is visible:

$$u_{\max} \approx \lambda \theta_0.$$

The linear variation of u_{\max} *versus* θ_0 can be deduced from the θ variation in the defect core if we postulate the molecules in the defect core as incompressible compared to the bulk compressibility of the smectic C* sample. In this case:

$$\begin{aligned} \frac{\partial u}{\partial z} &\approx (\cos\theta - \cos\theta_0) \approx \frac{1}{2} (\theta_0^2 - \theta^2) \\ u_{\max} &\approx \int_0^{2r} \frac{1}{2} (\theta_0^2 - \theta^2) dz \approx \frac{r\theta_0^2}{2} \tanh 2 \approx \frac{\mu\theta_0}{\sqrt{2}} \tanh 2 \approx \lambda\theta_0 \end{aligned}$$

The lower values of u_{\max} given by the numerical calculation close to $\theta_0 = 0$ correspond to a compression of the core due to the smectic C* bulk compressibility closer to the core compressibility in this case.

2.2.3. Azimuth Angle Variation. — The values of φ *versus* z and x for $\theta_0 = 0.1$ radian are plotted in the case of the parallel anchoring (Fig. 10) and of the symmetrical anchoring (Fig. 11). We can see that the φ distortion fills the sample. In Figure 13, φ is plotted *versus* z for different values of x around the defect; only a slight difference is visible between the calculated φ configuration and the values obtained in the constant θ approximation.

For the constant θ approximation the φ Euler equation reduces to a Laplace equation. An analytic expression is calculated in references [14] and [15]. We use the Fourier expansion of the φ variation in the \mathbf{xy} plane of the defect and we obtain in the bulk the expressions:

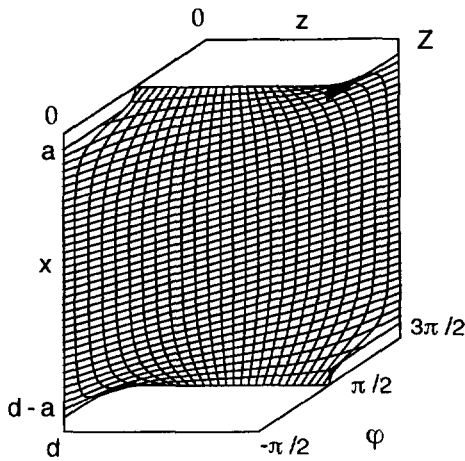


Fig. 10

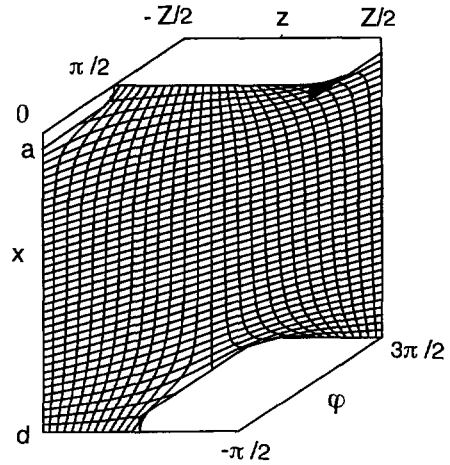


Fig. 11

Fig. 10. — Azimuthal angle of the molecules, φ , versus x and z in the case of parallel anchoring. The defect line corresponds to a jump of 2π of this angle. The drawing corresponds to one helical pitch.

Fig. 11. — Azimuthal angle of the molecules, φ , versus x and z in the case of symmetrical anchoring.

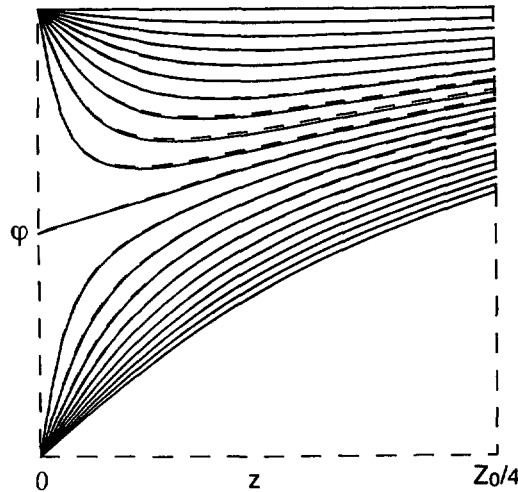


Fig. 12. — The azimuthal angle φ versus z for different distances x from the upper plate near the defect line. The continuous lines are the result of the computer calculation, the dashed lines are the constant θ approximation.

- for the parallel anchoring, $\varphi_1 = \varphi_2 = \pi/2$:

$$\varphi = \frac{\pi}{2} + 4 \sum_{p=0}^{\infty} \frac{\cos(2p+1) \frac{\pi a}{d} \sin(2p+1) \frac{\pi x}{d} \sinh(2p+1) \frac{\pi}{d} \left(z - \frac{Z}{2} \right)}{(2p+1) \sinh(2p+1) \frac{\pi Z}{2d}} \quad (1)$$

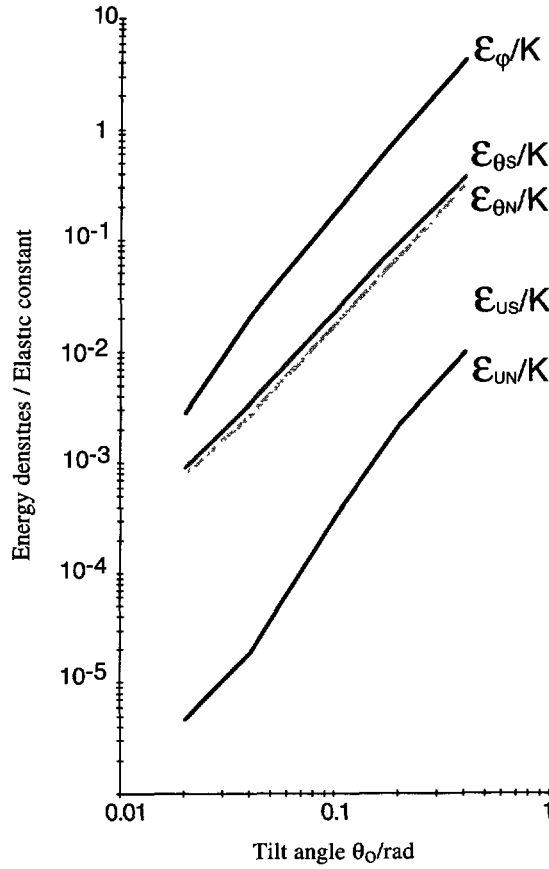


Fig. 13. — Energies of the line texture calculated for one pitch along z and one unit length along y , and reported to K , the nematic elastic constant. The computer calculation is made for $Z = Z_0 = d = 2 \mu\text{m}$, $\mu = 30 \mu\text{m}$ and $\lambda = 20 \mu\text{m}$. ϵ_{UN} = layer bend energy, ϵ_{US} = layer compression energy, $\epsilon_{\theta N}$ = nematic tilt energy, $\epsilon_{\theta S}$ = smectic tilt energy, ϵ_{ϕ} = total nematic azimuthal angle energy.

- for the symmetrical anchoring, $\varphi_1 = \pi/2, \varphi_2 = -\pi/2$ or $3\pi/2$:

$$\varphi = \frac{\pi}{2} + \frac{\pi x}{d} \frac{z}{|z|} + 2 \sum_{n=0}^{\infty} \frac{\cos n \frac{\pi a}{d} \sin n \frac{\pi x}{d} \left(\sinh n \frac{\pi Z}{d} - (-1)^n \sinh n \frac{\pi}{d} \left(z - \frac{Z}{2} \right) \right)}{n \sinh n \frac{\pi Z}{2d}} \quad (2)$$

- for the surface line case, $\varphi_1 = \varphi_2 = \pm\pi/2$:

$$\varphi = \frac{\pi}{2} + 2 \sum_{p=0}^{\infty} \frac{\sin(2p+1) \frac{\pi x}{d} \sinh(2p+1) \frac{\pi Z}{4d}}{(2p+1) \sinh(2p+1) \frac{\pi Z}{4d}} \quad (3)$$

The origin of x and z is on the first plate in the middle between the two defects near this plate. Z is the pitch of the helix in the middle of the sample. We will see in a following paragraph that Z can be slightly larger than Z_0 , the equilibrium helical pitch of the compound.

The agreement between the values of φ obtained with the constant θ approximation and with the numerical calculation is not surprising if we take into account the θ stability outside of the defect core established in the paragraph 2.2.1. This agreement is very interesting because it allows us to use the constant θ approximation to interpret the sample texture everywhere outside of the defect core.

2.2.4. Energy Considerations - Existence of the Defect Line Texture. — From the computer calculation, in the case of the line texture, we can obtain the different distortion energies of a sample. We calculate them for one pitch of the texture in the z direction and one unit length in the y direction. These energies divided by the elastic constant K are plotted in Figure 13 versus the tilt angle. The numerical calculation is made for a sample with parallel anchoring. The sample thickness is $2 \mu\text{m}$ and the helical pitch is $2 \mu\text{m}$.

We can see that the different energies are not at all equal. For a given θ_0 , the layer displacement energy ε_u is one order of magnitude lower than the molecular tilt angle energy ε_θ which is also one order of magnitude lower than the azimuth angle energy ε_φ . ε_{uN} , the layer bend energy is the lowest one; it increases very quickly with θ_0 . ε_{uS} , the smectic compression energy is more stable. The θ and φ energies vary roughly as θ_0^2 . We can see that the φ energy is not exactly proportional to θ_0^2 .

An estimation of the θ and φ energies can be made: for the bulk energy we saw that, out of the core, the φ configuration is very close to the one at θ constant, which follows a Laplace equation. The electrical analogy allows us to write the term of the out-of-core φ energy of a sample pitch as:

$$\varepsilon_{\varphi b} = 2\pi K\theta_0^2 \ln \frac{R}{r} = 2\pi K\theta_0^2 \ln \frac{R\theta_0}{\sqrt{2}\mu}$$

r is the defect core radius, or its expression from Section 2.2.1 and R is a given length close to the sample thickness or the helical pitch Z . R has to be independent of θ_0 . In the bulk, the two other terms are related to the spontaneous pitch Z_0 and are proportional to θ_0^2 . The logarithmic term induces the slightly more important variation of ε_φ with θ_0 .

For the core energies it is possible to calculate an approximate expression from the approximate expression of the configuration obtained when we assume the cylindrical symmetry defect:

$$\theta = \theta_0 \tanh \frac{\theta_0 \rho}{\sqrt{2}\mu} \quad \frac{\partial \varphi}{\partial \psi} = 1 \quad \frac{\partial \varphi}{\partial \rho} = 0$$

The origin is the defect center. ρ and ψ are the cylindrical coordinates. The core energies for the two lines in one pitch and one unit length in y are given by the integral:

$$\varepsilon_c = 2 \int_0^\pi \left\{ \underbrace{\frac{K\theta^2}{2} \left(\frac{1}{\rho} \frac{\partial \varphi}{\partial \psi} \right)^2}_{\varepsilon_{\varphi c}} + \underbrace{\frac{K}{2} \left(\frac{\partial \theta}{\partial \rho} \right)^2}_{\varepsilon_{\theta N}} + \underbrace{\frac{K}{4\mu^2} (\theta^2 - \theta_0^2)^2}_{\varepsilon_{\theta S}} \right\} 2\pi \rho d\rho$$

The different terms of this integral give

$$\varepsilon_{\varphi c} \approx 0.76\pi K\theta_0^2 \quad \varepsilon_{\theta N} = \varepsilon_{\theta S} = \pi K\theta_0^2 \frac{4 \ln 2 - 1}{3} \approx 0.59\pi K\theta_0^2$$

$\varepsilon_{\varphi c}$ is numerically calculated, $\varepsilon_{\theta N}$ and $\varepsilon_{\theta S}$ are analytically integrated. With these approximations, the two tilt energies $\varepsilon_{\theta N}$ and $\varepsilon_{\theta S}$ are equal.

We can compare these analytic results with the computer calculation given in Figure 13. The tilt nematic energy $\varepsilon_{\theta N}$ is exactly the same. The tilt smectic energy $\varepsilon_{\theta S}$ given by the

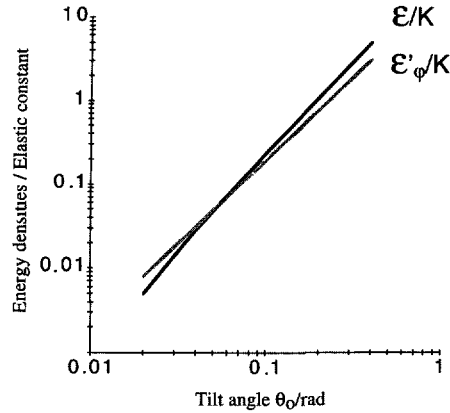


Fig. 14. — Total distortion energy ε for one pitch along \mathbf{z} and one unit length along the defect line (y) reported to K versus the tilt angle θ_0 . ε'_φ is the energy of the same area of the sample in the unwound state. The computer calculation is made for $Z = Z_0 = d = 2 \mu\text{m}$, $\mu = 30 \mu\text{m}$ and $\lambda = 20 \mu\text{m}$.

computer is 30% higher than the analytic approximation. The analytic approximation of ε_φ is questionable because it depends too much on the value of R which is not really defined.

To find the condition for the existence of the defect line texture, we have to compare its energy with the energy of the unwound state which is exactly:

$$\varepsilon'_\varphi = 2\pi^2 K \theta_0^2 \frac{dZ}{Z_0^2}$$

In Figure 14, ε'_φ and the total energy of the line texture, ε , are reported for $d = Z = Z_0 = 2 \mu\text{m}$. We can see that, for this thickness, the two energies are equal for $\theta_0 \approx 0.08$ radian, and the defect line texture is unstable if $\theta_0 > 0.08$ radian.

2.3. THE POSITION OF THE DEFECT LINES. — Near each plate a family of lines exists. The interaction between these two families and the plates is mainly due to the bulk φ distortion. We find the relative positions of the lines by minimizing the φ energy only, using the constant θ model. Indeed we saw that outside of the defect core the tilt angle is very close to the equilibrium tilt angle θ_0 . We first write the angle φ with a Fourier series in the general case when the defect line position is arbitrary. Then we calculate the φ energy ε_φ for one pitch in \mathbf{z} and one unit length in \mathbf{y} . The relative position of the two families of defect lines b and the distance a between a family and its neighbouring plate are calculated by minimizing ε_φ versus a and b .

The determination of the real pitch of the texture is more difficult than the two preceding calculations. Indeed we have to minimize the energy density versus the pitch; in this case the defect core energy as well as the bulk energy have to be taken into account.

2.3.1. General Expression of φ in the Constant θ Model. — For φ , the following expression can be obtained using the Fourier transformation, in the general case where the distance b between the two families of lines in the z direction (Fig. 3) is arbitrary.

- $b - Z/2 < z < Z/2$:

$$\varphi = \varphi_1 + (\varphi_2 - \varphi_1) \frac{x}{d} + 2 \sum_{n=1}^{\infty} \frac{\sin n \frac{\pi x}{d} \left(\cos n \frac{\pi a}{d} \sinh n \frac{\pi z}{d} - \cos n \frac{\pi(d-a)}{d} \sinh n \frac{\pi(z-b)}{d} \right)}{n \sinh n \frac{\pi Z}{2d}} \quad (4)$$

- $-Z/2 < z < b - Z/2$:

$$\varphi = \varphi_1 + (\varphi_2 - \varphi_1 - 2\pi) \frac{x}{d} + 2 \sum_{n=1}^{\infty} \frac{\sin n \frac{\pi x}{d} \left(\cos n \frac{\pi a}{d} \sinh n \frac{\pi z}{d} - \cos n \frac{\pi(d-a)}{d} \sinh n \frac{\pi(z+Z-b)}{d} \right)}{n \sinh n \frac{\pi Z}{2d}} \quad (4')$$

The origin is on plate 1, in the middle between two defects near this plate. Z is the pitch of the texture. φ_1 and φ_2 are the azimuth angle on the plates 1 and 2. In this expression the first part of the Fourier series gives the defect family 1 at the distance a from the plate 1; the second part gives the defect family 2 at the distance $-a$ from the plate 2 and shifted by b in the z direction with respect to the family 1.

The azimuth angle energy can be calculated in the form:

$$\varepsilon_\varphi = \frac{K\theta_0^2}{2} \int_{-z/2}^{z/2} dz \int_0^d dx \left\{ \left(\frac{\partial \varphi}{\partial x} \right)^2 + \left(\frac{\partial \varphi}{\partial z} \right)^2 - \frac{4\pi}{Z_0} \left(\frac{\partial \varphi}{\partial x} \sin \delta + \frac{\partial \varphi}{\partial z} \cos \delta \right) + \frac{4\pi^2}{Z_0^2} \right\} \quad (5)$$

Here we take into account an eventual tilt of the smectic layer (Fig. 30). δ is the angle between the layer normal and the z axis. A simple calculation gives the result:

$$\frac{\varepsilon_\varphi}{K\theta_0^2} = 4\pi \sum_{n=1}^{\infty} \frac{\cos^2 n \frac{\pi a}{d} \left(\cosh n \frac{\pi Z}{2d} - (-1)^n \cosh n \frac{\pi(Z-2b)}{2d} \right)}{n \sinh n \frac{\pi Z}{2d}} + \frac{2\pi b(\pi - \varphi_2 + \varphi_1)}{d} \quad (6)$$

$$+ \frac{Z(\varphi_2 - \varphi_1)^2}{2d} - 2\pi \frac{[Z(\varphi_2 - \varphi_1) - 2\pi b] \sin \delta + 2\pi(d-2a) \cos \delta}{Z_0} + \frac{2\pi^2 Z d}{Z_0^2}$$

2.3.2. Relative Position of the Two Defect Families. — The derivation of ε_φ/Z versus b gives the force in the z direction applied on a unit area of one family of defects by the other family. This force by unit area is a shear.

$$-\frac{\partial \varepsilon_\varphi}{\partial b} \frac{1}{Z} = -\frac{4\pi^2 K \theta_0^2}{Zd} \left(\underbrace{\sum_{n=1}^{\infty} \frac{(-1)^n \cos^2 n \frac{\pi a}{d} \sinh n \frac{\pi(Z-2b)}{2d}}{\sinh n \frac{\pi Z}{2d}}}_{p_1} + \underbrace{\frac{(\pi - \varphi_2 + \varphi_1)}{2\pi}}_{p_2} + \underbrace{\frac{d \sin \delta}{Z_0}}_{p_3} \right)$$

In Figure 15, the shear between the two line families (p_1 , the sum of the series) is plotted versus b and for three different values of the sample thickness. This shear is symmetrical with respect to $b = Z/2$ and tends to put the two families in alternate position. We can remark

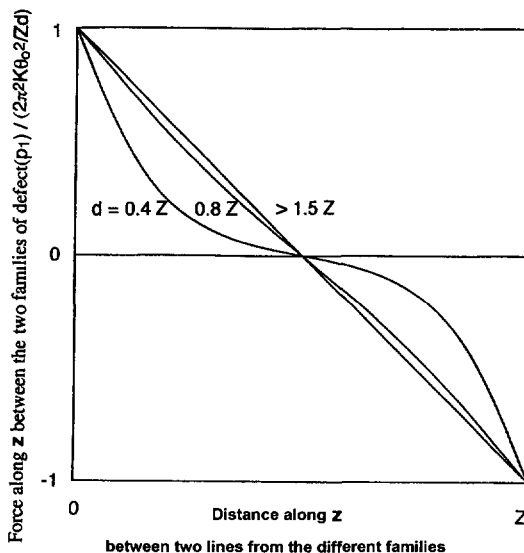


Fig. 15. — Force, p_1 , in the z direction applied by a defect line family, close to one plate, on unit area of the second line family close to the other plate. This force is calculated *versus* b for different thicknesses d of the sample. b is the distance along z between two lines from different families. The distance in the x direction from one family of line to its neighbouring plate is the equilibrium distance: $a = Z/4\pi$.

that for thin samples close to $b = Z/2$ the shear is very weak. For thick samples ($d \gg 1.5 Z$), Figure 16 shows that p_1 can be approximated by a linear law, and the equilibrium equation gives the value of b in the form:

$$b = \frac{Z_0}{\cos \delta} \frac{\varphi_2 - \varphi_1}{2\pi} - d \tan \delta \quad \text{because} \quad Z = \frac{Z_0}{\cos \delta}$$

The two other shears do not vary with b . One is the effect of the different anchoring on the two surfaces; this shear vanishes for $\varphi_2 - \varphi_1 = \pi$, the symmetrical anchoring, and tends to increase b if $\varphi_2 - \varphi_1 > \pi$. The last shear is related to the tilt of the layer, it tends to decrease b if $\delta > 0$. The defects are pushed by the layer tilt. They try to stay in the same layer.

When the layers are perpendicular to the plates ($\delta = 0$), two particular cases are very common. For the symmetrical anchoring $\varphi_2 - \varphi_1 = \pi$ all the three shears vanish for $b = Z/2$, and the two line families are alternate, as drawn in Figure 3b; this alternate position is better defined in thick samples. For the parallel anchoring $\varphi_1 = \varphi_2$, the anchoring tends to lower b . The equilibrium is obtained for $b = 0$ and the two line families are in phase as drawn in Figure 3a; this position is better defined for thin samples.

When the layers are tilted ($\delta \neq 0$) in the case of parallel anchoring, the pairs of lines from the two families are in the same smectic layer (at the foot of Fig. 30, $\delta > 0$). In the case of symmetrical anchoring, (at the top of Fig. 30, $\delta < 0$), the tilt of the layer and the difference between the two anchoring angles can put the lines of the two families in front of each other.

2.3.3. *Position of the Lines with Respect to the Plates.* — Using the previous energy expression, we can evaluate the position of the defect lines with respect to the neighbouring plate. We

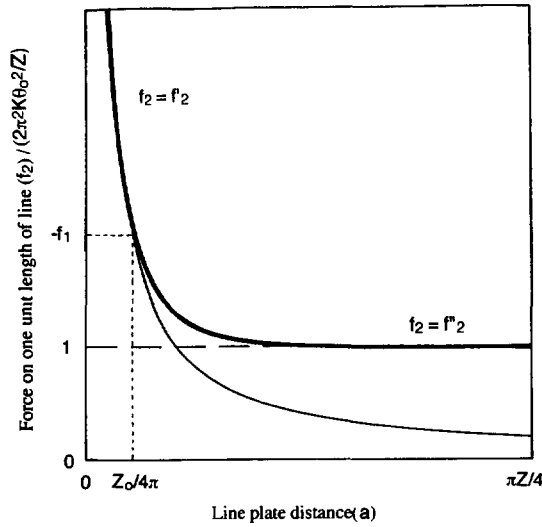


Fig. 16. — Force, f_2 , per unit length on a defect line, due to the interaction with all the other lines and the plates, in the case of thick samples ($d > \pi Z$). For comparison the thin line, f'_2 is the force on the line due to its image by the neighbouring plate; the interrupted line, f''_2 is the force per unit length due to a continuous layer made by the images of the lines of its family. f_1 is the force due to the helix.

derive $\varepsilon_\varphi/2$ with respect to a to find the force in the x direction on one unit length of one defect.

$$-\frac{\partial \varepsilon_\varphi}{\partial a} \frac{1}{2} = f_1 + f_2$$

with

$$f_1 = \frac{-4\pi^2 K \theta_0^2}{Z_0} \cos \delta \quad \text{and}$$

$$f_2 = -2\pi K \theta_0^2 \frac{\partial}{\partial a} \sum_{n=1}^{\infty} \frac{\cos^2 n \frac{\pi a}{d} \left(\cosh n \frac{\pi Z}{2d} - (-1)^n \cosh n \frac{\pi(Z-2b)}{2d} \right)}{n \sinh n \frac{\pi Z}{2d}}$$

The term f_1 can be interpreted as a constant force due to the helix. This force tends to repel the defects toward the plates to obtain a perfect helix throughout the whole sample. The series term f_2 is the force applied on the defect lines by the plates and the other defects. This force repels the line from the plate. In Figure 16 is plotted f_2 versus a for a very thick sample ($d \sim \infty$). In comparison we have also plotted f'_2 the force applied on one line by its image due to the neighbouring plate and f''_2 , the force applied on one line by a continuous layer made by the image lines of its family.

$$f'_2 = \frac{\pi K \theta_0^2}{a} \quad f''_2 = \frac{2\pi^2 K \theta_0^2}{Z}$$

- If a is smaller than $Z/4\pi$, $f_2 \approx f'_2$, this means that the line is close to the plate, the force on one line is only the force due to its image. This force is proportional to $1/a$.

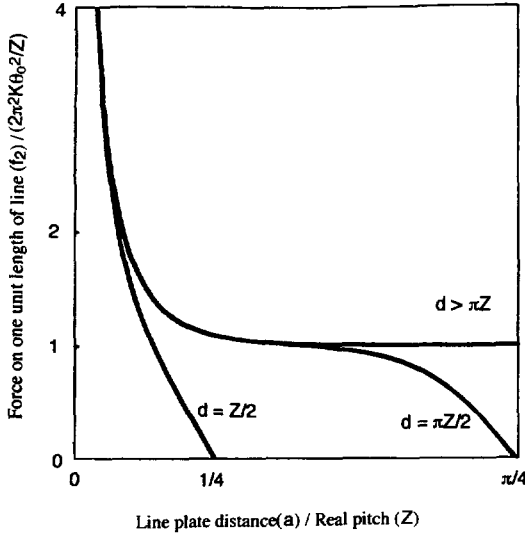


Fig. 17

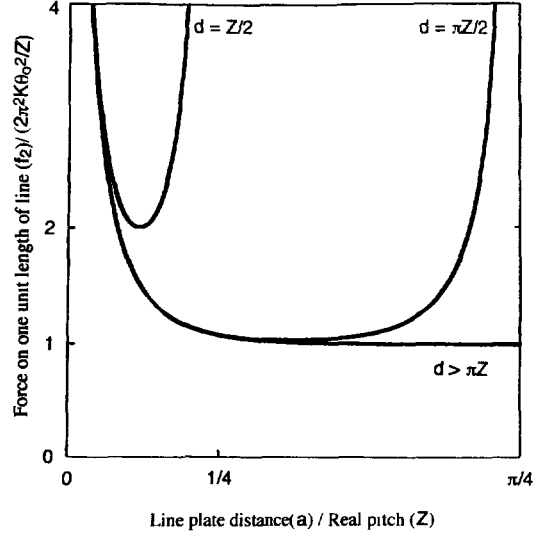


Fig. 18

Fig. 17. — Force, f_2 , per unit length on one defect line *versus* its distance a from its neighbouring plate for different values of the sample thickness, d . The calculation is made when the two families of lines are in alternate position and at the same distance from their neighbouring plates. As a symmetry argument allows to predict, when the two families are in the same plane ($a = d/2$), f_2 vanishes.

Fig. 18. — Force, f_2 , per unit length on one defect line, *versus* its distance a from its neighbouring plate, for different values of the sample thickness, d . The calculation is made when the two families are in front of each other and at the same distance from their neighbouring plates. When the line is close to that in front of it ($a \sim d/2$), the force diverges and the two lines vanish.

- If a is larger than Z/π , $f_2 \approx f_2''$, the force on one line is the force due to all the images of its family, seen as a continuum. This is a constant force equal to $2\pi^2 K \theta_0^2 / Z$. The position of the line corresponds to the equilibrium between these two forces f_1 et f_2 :

$$\frac{4\pi^2 K \theta_0^2}{Z_0} \equiv -f_1 = f_2 \approx f_2' \equiv \frac{\pi K \theta_0^2}{a} \quad \text{so} \quad a = \frac{Z_0}{4\pi}$$

Indeed we will see that every time the real pitch of the texture is larger than the spontaneous pitch, so the condition for the approximation is satisfied ($a < Z/4\pi$).

For a thin sample, we can see in Figures 17, 18 the effect on f_2 of the thickness d in two cases: the parallel anchoring where the two line families are just in phase and the symmetrical anchoring where they are alternate.

- For the symmetrical anchoring, the lines of the other family are far; their influence is very small. The force f_2 vanishes when the line is in the middle of the sample because of the image line due to the other plate. An equilibrium position exists for every thickness of the sample, a decreases with d but stays close to $a = Z_0/4\pi$.
- For the parallel anchoring, the line is just in front of a line from the other family. As shown in Figure 18, the other line pulls the line toward the sample center, increasing f_2 . The two lines tend to annihilate because the force f_2 tends to infinity when the lines tend

one to the other. The curve of f_2 is symmetrical with respect to $a = d/4$. In practice a stays close to $Z_0/4\pi$ so long as d is larger than a critical value. This can be calculated if we take into account only the interaction of the line with its image and the line in front of it. The critical value of d corresponds to the case where the helical force is just opposite to the lower value of the line force.

$$\pi K \theta_0^2 \left(\frac{1}{a} + \frac{2}{d-2a} \right) = \frac{4\pi^2 K \theta_0^2}{Z_0} \quad \text{and} \quad a = \frac{d}{4}$$

give the critical thickness value:

$$d_c = \frac{2Z_0}{\pi}$$

The computer calculation takes into account all the lines and gives: $d_c \approx Z_0/2$. So for this anchoring, the line texture cannot appear for a thin sample ($d < Z_0/2$).

2.3.4. Real Pitch of the Line Texture. — We will make the calculation when the molecules lie parallel on the two plates and when the smectic layers are perpendicular to the plates; this will allow us to compare the calculation with an experimental result.

The equilibrium equation for the pitch Z is:

$$\frac{\partial}{\partial Z} \left(\frac{\varepsilon}{Z} \right) = -\frac{\varepsilon_{\theta N} + \varepsilon_{\theta S} + \varepsilon_{\varphi c}}{Z^2} + \frac{\partial}{\partial Z} \left(\frac{\varepsilon_{\varphi b}}{Z} \right) = 0$$

For the defect core energies $\varepsilon_{\theta N}$, $\varepsilon_{\theta S}$ and $\varepsilon_{\varphi c}$ we postulate that they are independent of the pitch Z and of the sample thickness d . This is realistic because Z and d are much larger than the core radius r in every case except very close to the A-C transition. For these energies, we will use the computer calculation.

The bulk energy is only the azimuth angle energy. We take for φ expression (1) and for ε_{φ} expression (5), but, to keep only the bulk energy and avoid the series divergence, we integrate for $-Z/2 + r \leq z \leq Z/2 - r$. We then obtain:

$$\frac{\varepsilon_{\varphi b}}{\pi K \theta_0^2 Z} = \frac{4}{Z} \sum_{p=0}^{\infty} \frac{\cos^2(2p+1) \frac{Z_0}{4d} \sinh(2p+1) \frac{\pi(Z-2r)}{d}}{(2p+1) \sinh^2(2p+1) \frac{\pi Z}{2d}} - \frac{4\pi d - 2Z_0}{Z_0 Z} + \frac{2\pi d}{Z_0^2} \quad (6')$$

The derivative of this expression inserted in the pitch equilibrium equation gives the equation which links d , Z and Z_0 with the core energies:

$$\frac{2\pi d'}{Z_0} = 1 + \frac{\varepsilon_{\theta N} + \varepsilon_{\theta S} + \varepsilon_{\varphi c}}{2\pi K \theta_0^2} + 2 \sum_{p=0}^{\infty} \frac{\cos^2(2p+1) \frac{Z_0}{4d} \left\{ (2p+1) \frac{\pi Z}{d} + \sinh(2p+1) \frac{\pi(Z-2r)}{d} \right\}}{(2p+1) \sinh^2(2p+1) \frac{\pi Z}{2d}}$$

In this form the equation can be solved by a relaxation method: we fix a value for Z/d and inject in the series the same value for Z_0/d , the equation gives a new value for Z_0/d that is re-injected.

The core energies have been obtained in paragraph 2.2.4.

$$\frac{\varepsilon_{\theta N} + \varepsilon_{\theta S} + \varepsilon_{\varphi c}}{2\pi K \theta_0^2} \approx 0.97 \approx 1.08 \approx 1.16$$

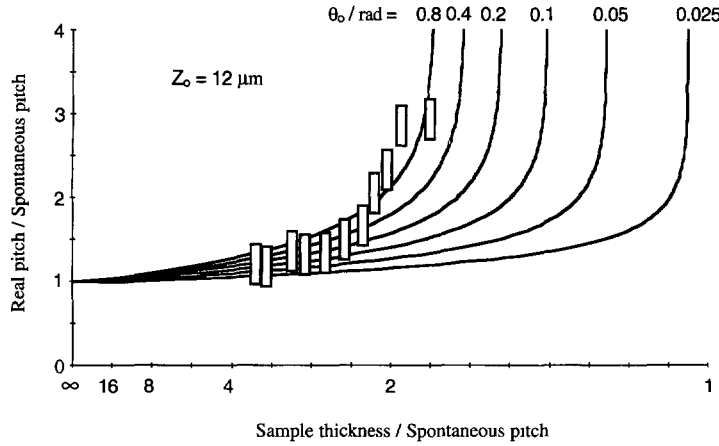


Fig. 19. — Real pitch Z versus the sample thickness d reported to the spontaneous pitch Z_0 for different tilt angle in radian. The rectangles are measured values for $\theta_0 = 0.78$ radian.

The first value corresponds to the analytical approximation, the computer gives the two following values for $\theta_0 = 0.1$ and 0.4 radian; the values are the same for $Z = Z_0 = d = 2 \mu\text{m}$ or $Z = Z_0 = 2 \mu\text{m}$ and $d = 3.14 \mu\text{m}$. We take 1 as a realistic value for this expression.

In Figure 19 the pitch Z is plotted versus the sample thickness d . The different curves correspond to six values of the tilt angle θ_0 . When $d \gg Z_0$, $Z = Z_0$, the central part of the sample is in its minimum energy state. If the sample thickness decreases, the pitch increases to lower the energy by lowering the number of defects. We can notice for example that for $\theta_0 = 0.8$ radian and $d = 5Z_0$ the pitch is 20% higher than the spontaneous pitch. For thin samples the pitch diverges because the energy of the defects is higher than the energy gain due to a helical central part: the sample is unwound.

In Figure 20 the critical thickness d_c is plotted versus θ_0 , for $Z_0 = 2 \mu\text{m}$ and $Z_0 = 12 \mu\text{m}$; the calculation is made with the series equation. d_c increases with θ_0 because of the r logarithmic term in the bulk φ energy that increases the energy of the line texture more than the unwound one. In the pitch equilibrium equation, if Z tends towards infinity the series can be integrated; in addition if we consider $4\pi r \ll Z_0 < 4d$, we obtain for d_c the equation:

$$\frac{2\pi d_c}{Z_0} - 2 \ln \frac{d_c}{Z_0} = 1 + \frac{\varepsilon_{\theta N} + \varepsilon_{\theta S} + \varepsilon_{\varphi c}}{2\pi K \theta_0^2} + \ln \frac{4Z_0}{\pi\sqrt{2}\mu} + \ln \theta_0$$

The difference between the result of this equation and d_c plotted in Figure 20 is only one per cent.

We can compare the minimum thickness of the helical texture obtained here, by divergence of the pitch, with the two other determinations. In paragraph 2.3.3, for the parallel anchoring, the lines annihilate if $d < Z_0/2$; this gives a lower limit of the helical texture critical thickness: $d_c > Z_0/2$. In paragraph 2.2.4, we saw that if $d = Z = Z_0 = 2 \mu\text{m}$ and $\theta_0 = 0.08$ rad, the helical texture and the unwound one have equal energies; for this thickness the energy density of the structure can be lowered by increasing its real pitch and the structure remains stable. This gives an upper limit for the helical texture thickness: $d_c < Z_0$. The equation gives $d_c = 0.9Z_0$ if $\theta_0 = 0.08$ rad and $Z_0 = 2 \mu\text{m}$. This value is close to its upper limit.

In Figure 19 the experimental measurements (Sect. 3.1.2) of the real pitch of an edge sample are reported versus its thickness. For this sample $\theta_0 = 45^\circ \approx 0.8$ radian and the spontaneous

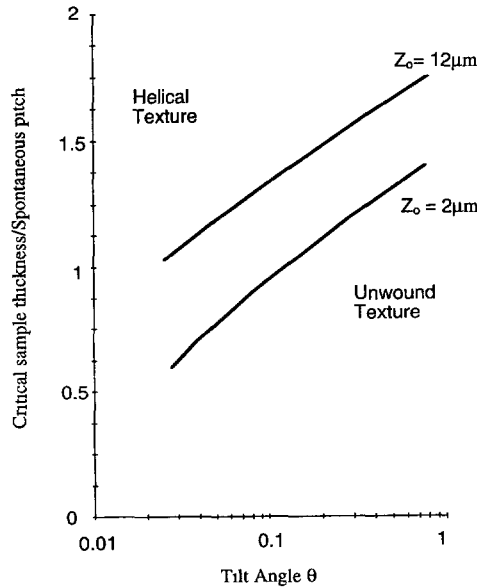


Fig. 20. — Critical sample thickness d_c reported to the spontaneous pitch Z_0 versus the molecular tilt angle θ_0 in radian, for two spontaneous pitches.

pitch measured by the Grandjean-Cano method is $15 \mu\text{m}$. The error rectangles correspond to the dispersion in the sample. For the theoretical curves the only adjustable parameter used is the spontaneous pitch and the best fit corresponds to $Z_0 = 12 \mu\text{m}$. If we take into account the uncertainty about the smectic elastic constants, we can say that the experiment confirms our calculation of the defect core energy and thus the hypothesis of an $A - C^*$ transition in the defect line.

3. Experimental Situation in Limited Sample Textures

3.1. LINE POSITION. — Surface lines are very uncommon but, when they exist, they are very often connected to a bulk line. Photo 2 (p. 1713) shows an unwinding volume line becoming two surface lines. In the Figure 21 the area located between the two surface lines is black with crossed polarizers while the other part of the background is black when the angle between the polarizer and the analyser is about 60° . This difference shows that the anchoring directions on the glasses are different on each side of a line. Figure 22 shows the distribution of the director in this case.

Generally unwinding lines are not surface lines and in reference [4] it has been said that the distance between the glass plate and the line is about half the spontaneous pitch Z_0 . Here we report the results of measurements of this distance in relation to the spontaneous pitch.

3.1.1. *Line-Plate Distance versus Sample Thickness: Measurement Method.* — The method of measurement requires a wedge-shaped geometry for the sample. Straight sharp ink lines perpendicular to the edge are drawn on the glass plates. In this way it is possible to measure the thickness of the sample in a given place, by focusing with a large magnification on the upper mark and then on the lower one. The slow displacement of the stage, which gives fine focusing, is graduated, so vertical distances can be measured. The difference between the two

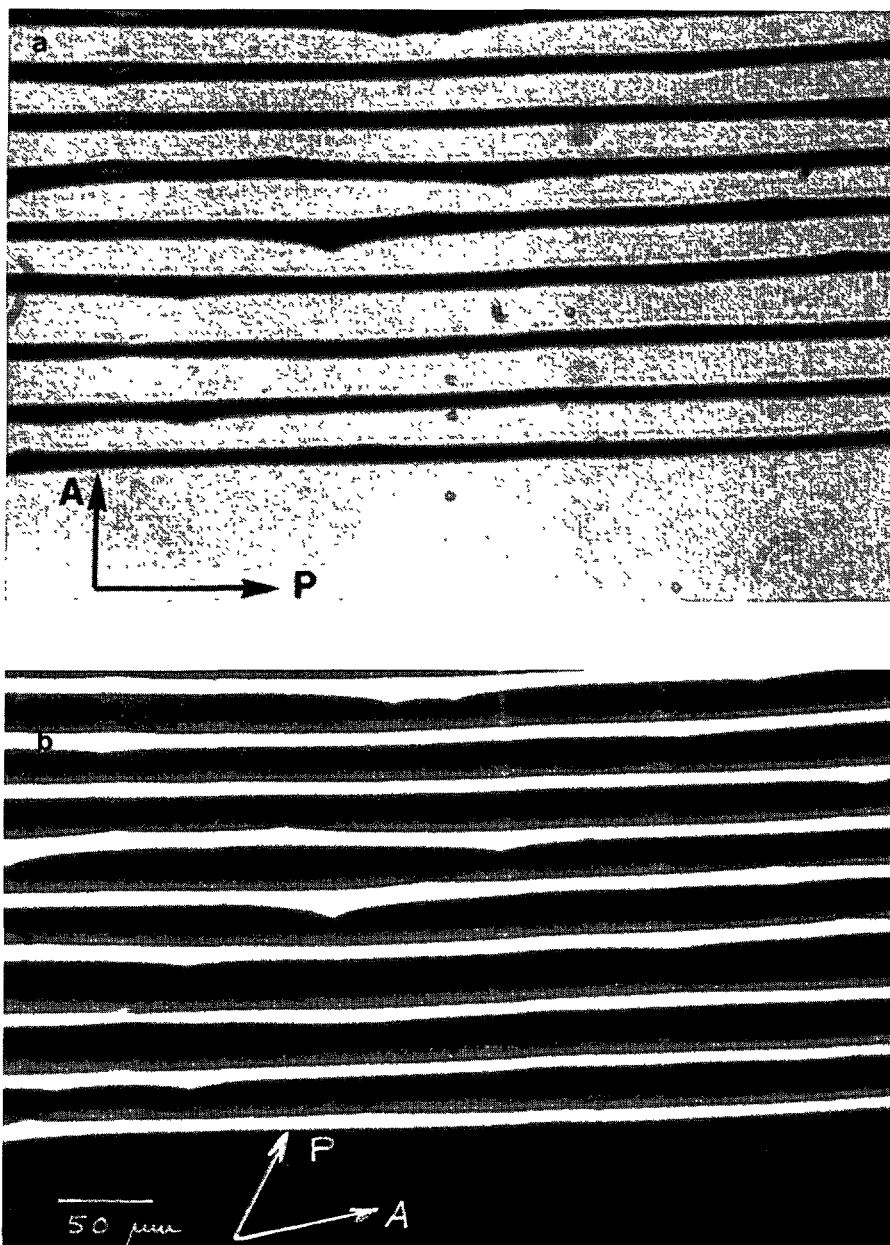


Fig. 21. — a) The area located between the two surface lines is black with crossed polarizers. b) The part of the background located out of the surface lines is black when the angle between the polarizer and the analyzer is about 60° . This difference shows that the anchoring directions on the glasses are different between a couple of surface lines and outside. Same experimental conditions as in Photo 2 (p. 1713), except polarizer positions.

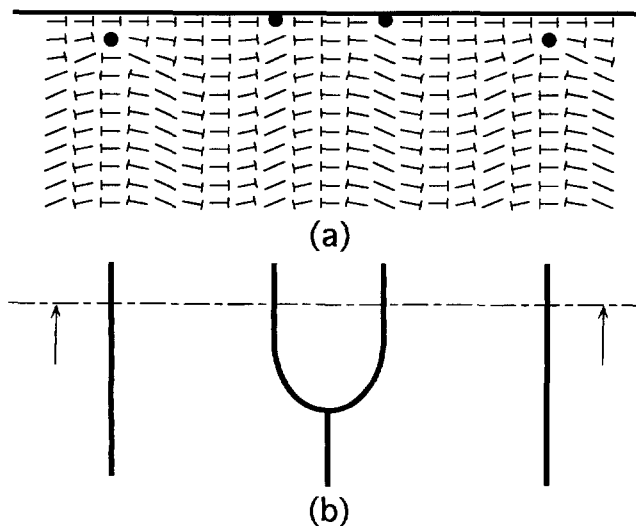


Fig. 22. — The director distribution in the case where one volume lines becomes two surface lines.

readings indicates the apparent thickness, d_a . The true thickness, d , is $d_a n$, n being the average refractive index. d can be calculated from the shape of the wedge as a function of the distance between the zero thickness point and the point where the measurement is made, or can be measured when the cell is empty. d/d_a gives a good estimation of n . Then, in the place where the unwinding lines are located, the apparent distance between the surface and the unwinding lines is measured, focusing on it or on ink lines, and multiplying by n , the situation of the unwinding lines in the sample is deduced. The best accuracy of the measurement is only one to two microns.

3.1.2. Superimposed Lines, Parallel Anchoring

3.1.2.1. Line — Plate Distance. — Generally the spontaneous pitch of pure compounds is about $2 \mu\text{m}$ to $5 \mu\text{m}$. To do significant measurements, it is necessary to use compounds the pitch of which is larger than the average pitch of pure compounds. In reference [1], we had used a mixture of a non-chiral smectic C (bis-4'-n-decyloxybenzal-2-chloro-1-4-phenylene diamine-D.O.B.C.P.) with cholesteryl cinnamate, a cholesteric liquid crystal. This mixture for a concentration of 5% in cholesteryl cinnamate has a pitch of $15 \mu\text{m}$ and a tilt angle $\theta_0 = 45^\circ$; it gives superposed lines [4]. In the present work, we have used the same mixture, at several concentrations it presents the same θ_0 but as expected the pitch varies. The pitch measurements by the Grandjean-Cano method give for the different concentrations: 6%, $Z_0 = 12.5 \mu\text{m}$, 3%, $Z_0 = 25 \mu\text{m}$, 1.77%, $Z_0 = 42 \mu\text{m}$.

The plate-line distances, a , calculated from measurements with $n = 1.5$ are respectively about $1-2 \mu\text{m}$, $3 \mu\text{m}$, $5 \mu\text{m}$. These values, because of the weak precision of the measurements, indicate essentially that the line-plate distance is proportional to the spontaneous pitch and the order of magnitude is about $Z_0/6$ to $Z_0/10$. Moreover the distance line-plate does not vary when the sample thickness varies. It is independent of d , and is the same for the two glass plates.

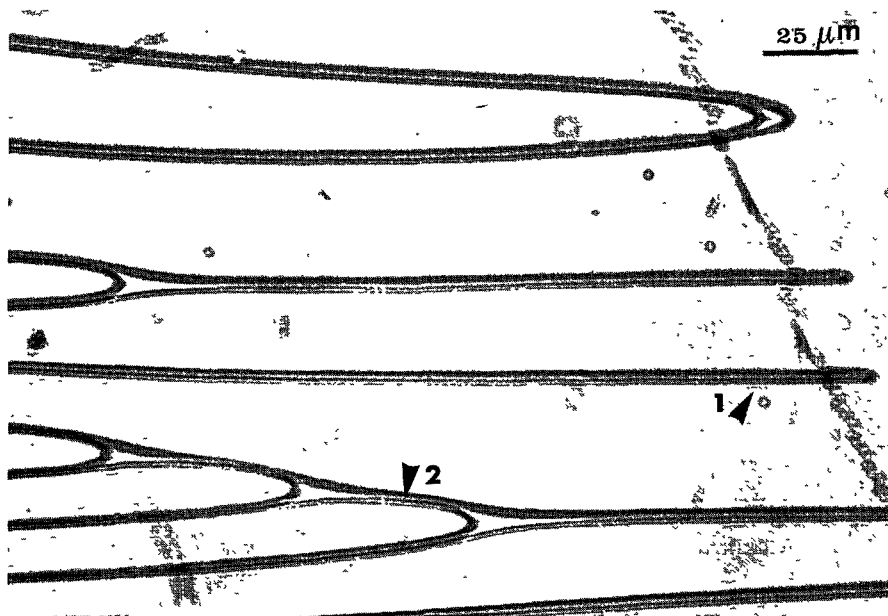


Fig. 23. — Where the cell thickness is of the order of the pitch Z_0 the two lines of a pair collapse (arrow n°1) or sometimes the upper line of a pair collapses with the lower line of the neighbouring pair (arrow n°2). Compound: a 5% mixture of cholesteryl cinnamate with bis-(4'-n-decyloxybenzyl) 2-chloro-1-4-phenylenediamine. The anchoring direction induced by the SiO evaporation makes an angle 45° with the edges of the photo. Polarizer is perpendicular to the anchoring direction. No analyser.

When two superposed lines come closer to another they collapse, as implied by the theory. In this case a loop made by such a pair of lines vanishes when their distance becomes of the order of the pitch Z_0 (Fig. 23).

Thus for superposed lines, that is to say when bounding molecules are parallel, the distance a is not dependent on the sample thickness, d , but is dependent on the pitch Z_0 and is of the order of $Z_0/8$. This is not too far from the value $a = Z_0/4\pi$ given by the theoretical calculation of Section 2.3.3.

3.1.2.2. Relative Position of the Two Lines of a Pair. — The relative position of the lines is dependent of the anchoring directions on the surfaces. Using a topological argument we have already described the parallel anchoring as giving superposed lines [4]. In Figure 1 the polarizer and analyser are crossed, parallel and perpendicular to the anchoring direction on the surface. Between the lines the background is really black. That is a proof of the parallel anchoring. In this case, as we can see in Photo 3 (p. 1713), the lines forming two families near both plates are superposed. Only some accidents like dust introduce a slight shift. As in the previous paragraph this result is consistent with the elastic theory which predicts that the two lines of a pair are located one in front of the other in the same smectic layer.

3.1.2.3. Distance Between Two Lines of the Same Family: The Helical Pitch. — The distance between two lines of the same family is said to give the value of the pitch of the helix. Very often in the same sample, this distance is not a constant [16]. It would be better to say that

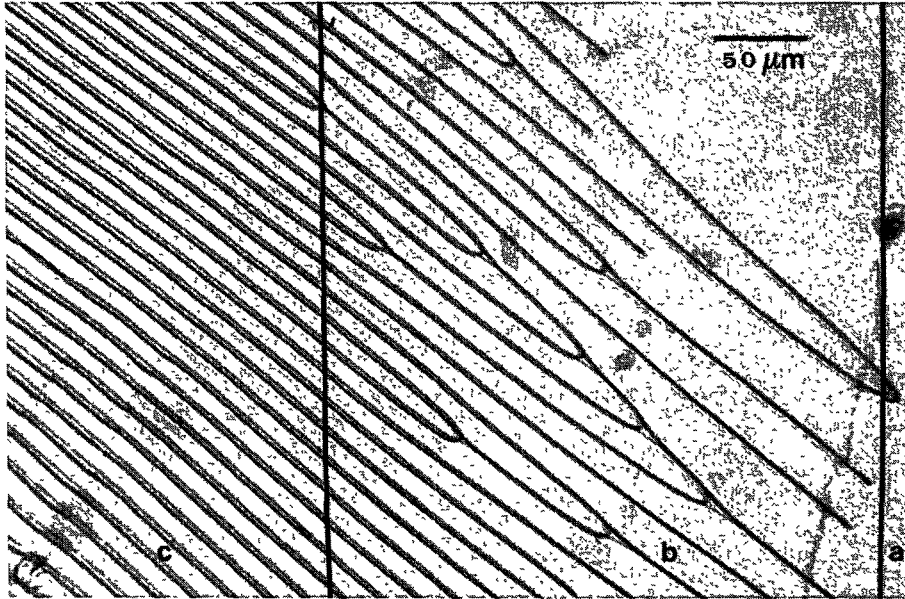


Fig. 24. — Superposed lines in a cylindrical geometry. Compound: a 5% mixture of cholesteryl cinnamate with bis-(4'-n-decyloxybenzal) 2-chloro-1-4-phenylenediamine. Aligning layer: 60° evaporated SiO. Polarizer is parallel to the aligning direction and makes an angle 45° with the edge of the photo. No analyzer. In the part noted a), d is $\lesssim Z_0$, there is no line at all. In the part noted c), d is $\gtrsim 5Z_0$, the distance between two neighbouring lines is the normal pitch, Z_0 . In the part noted b), $Z_0 < d \lesssim 5Z_0$, the distance between two neighbouring lines, always $> Z_0$, is called the local pitch, Z .

the value deduced from the distance measurement gives the local pitch. To determine the equilibrium pitch we have measured the helical pitch for the mixture of cholesteryl cinnamate in DOBCP (5%) by the Grandjean-Cano method. The spontaneous pitch of the S_C^* structure Z_0 , far from the transition $N^* - S_C^*$ is found by this method to be 15 μm .

Photo 1. — The texture of a chiral smectic C between two untreated glass plates: the direction of the lines indicates the direction of the smectic layers. Compound: 4-methyl hexyloxyphenyl decyloxybenzoate. Cell thickness: about 30 μm . Crossed polarizers.

Photo 2. — Superposed lines where each line situated near one of the surfaces is transformed into two neighbouring surface lines (arrow n°1) which are sharp in the photo. The lines situated near the other surface are blurred (arrow n°2). Compound: ZLI 3488 from Merck. The pitch is about 12 μm . Polarizers are in any position. Scale: 1 cm = 50 μm .

Photo 3. — Superposed lines. Some "accidents" produce a slight shift of the lines. The focus is made on the upper lines (arrow n°1). Focal conics (arrow n°2) indicating some variation in the direction of the layers are located in the bulk. The cell thickness is about 50 μm . Compound: a 3% mixture of cholesteryl cinnamate with bis-(4'-n-decyloxybenzal) 2-chloro-1-4-phenylenediamine. Polarizers in any position. Aligning layer: 60° evaporated SiO. Scale: 1 cm = 25 μm .



Photo 1

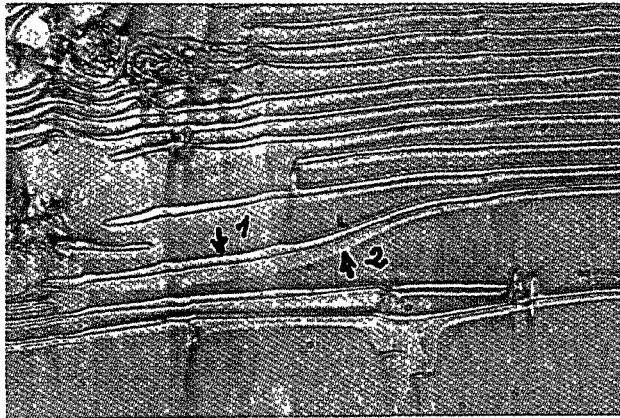


Photo 2

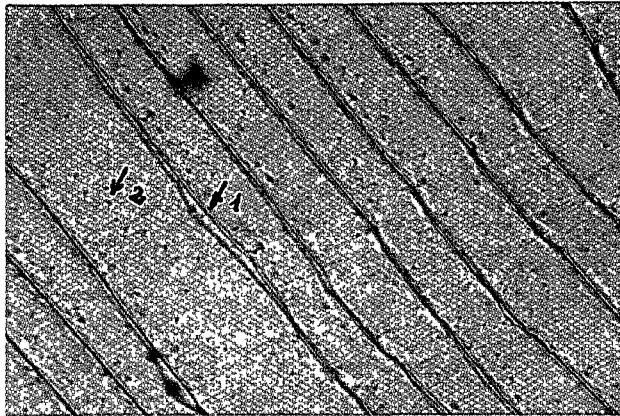


Photo 3

To evaluate the relation between the cell thickness, d , and the local pitch we have observed the unwinding lines in the cylindrical geometry (between a flat glass and a cylindrical lens). The Figure 24 shows that:

- where $d \lesssim Z_0$ there is no line at all;
- where $d \gtrsim 5Z_0$ the distance along z between two neighbouring lines gives the equilibrium pitch Z_0 ;
- where $Z_0 \lesssim d \lesssim 5Z_0$, the z distance is always $> Z_0$. We call this distance the local pitch Z . In this region we have measured Z with respect to d . The results of these measurements are the rectangles in Figure 19 giving Z/Z_0 as a function of d/Z_0 . Here too our experimental results are close to the results given by the calculation (Sect. 2.3.4): the best fit corresponds to a spontaneous pitch of $12 \mu\text{m}$ and the measurements by the Grandjean-Cano method give $Z_0 = 15 \mu\text{m}$.

In conclusion, for parallel anchoring, the measured values of the line-plate distance of the pitch Z in relation with d and the relative position of the two families of lines are in good agreement with the values deduced from the theory.

3.1.3. Shifted Lines, Symmetrical Anchoring

3.1.3.1. Line Plate Distance. — To measure this distance we also had to use mixtures in order to increase the pitch. But because of the weak precision, we thought unnecessary to do several concentrations.

Measurements have been made with a mixture of DOBAMBC and its racemic (50%) the pitch of which, measured by the Grandjean-Cano method, is equal to $10 \mu\text{m}$. The texture is dependent on the sample thickness.

- When the thickness is smaller than about twice the spontaneous pitch one lattice (Photo 4, p. 1715) of shifted lines is in place. In this case the space between the upper and the lower line does not occupy the whole sample thickness. Only one line is located near the glass plate, with a distance a which is of the order of 1 to $2 \mu\text{m}$. It can be located either near the upper glass plate or near the lower one. The distance between the other line and the surface is variable. For example, in a place where the sample thickness is $21 \mu\text{m}$, the distance between the line and the plate is about $1 \mu\text{m}$ the distance between both lines about $12 \mu\text{m}$. So, the distance between the second line and the second plate is $8 \mu\text{m}$. Why does a pair of lines not occupy the whole sample thickness? According to the elastic theory we have found (Sect. 2.3.3) that the equilibrium position of the two lines of a pair is located at the distance $a \approx Z_0/12$ from the nearest plate. It seems as though there was a rigid wall in the cell which prevents one line from going close to the plate.
- When the sample thickness is larger than twice the spontaneous pitch, one always observes lines located in three different levels:
 - * one family near the upper glass plate (Photo 5a, p. 1716);
 - * another family located on an intermediate level, whose lines are put closer together (Photo 5b, p. 1716);
 - * a third family, similar to the first one, near the lower glass plate (Photo 5c, p. 1716). However with a strong magnification, the intermediate level can be separated into two levels, the distance of which, along x , is of the order of twice the distance

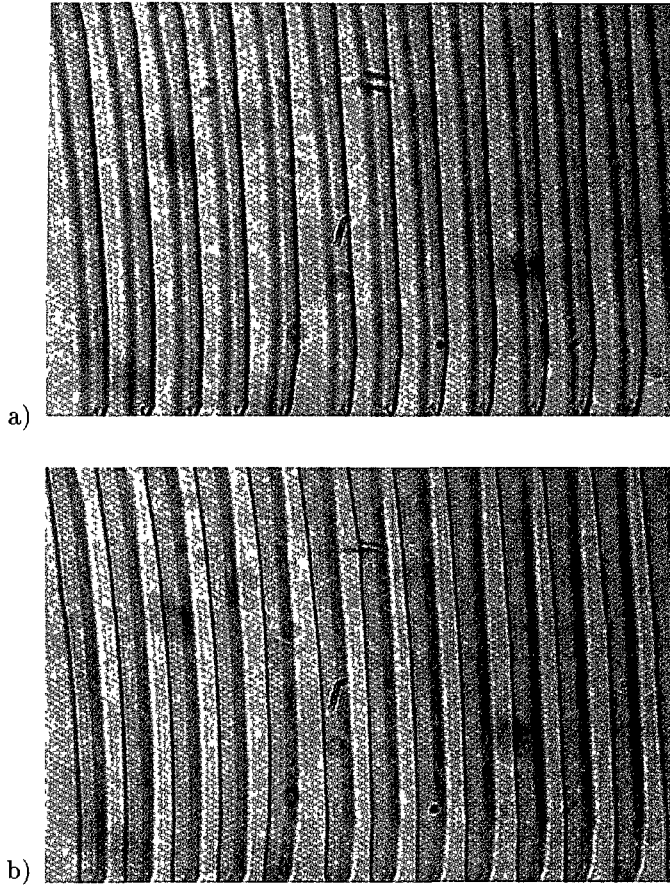


Photo 4. — Pairs of shifted lines when the cell thickness is less than twice the pitch: a) Focus on the lines located near the upper plate. b) Focus on the lines located in the bulk of the cell, approximately in the middle. Compound: a 50% mixture of chiral p-decyloxybenzylidene p'-amino 2-methyl butyl cinnamate (D.O.B.A.M.B.C.) with the racemic. Polarizers are in any position. Scale: 1 cm = 20 μm .

between one line and the plate. For example in a place where the sample thickness is 40 μm :

- distance plate 1 - line 1 is about 1 μm ,
- line 1 - line 2, about 19 μm ,
- line 2 - line 3, about 2 μm ,
- line 3 - line 4, about 16 μm ,
- line 3 - plate 2, about 1 μm .

We can conclude that two lattices of pairs of lines are superposed. Tsuchiya *et al.* [17] also observed more than two families of lines they described as bulk lines and surface lines. Nothing in the theory can explain this phenomena. We have seen that in the case of parallel anchoring the equilibrium state for the position of the lines with respect to the plates is only dependent on Z_0 ($a \sim Z_0/12$).

Everything happens as if a wall was dividing the sample into independent parts. What is the

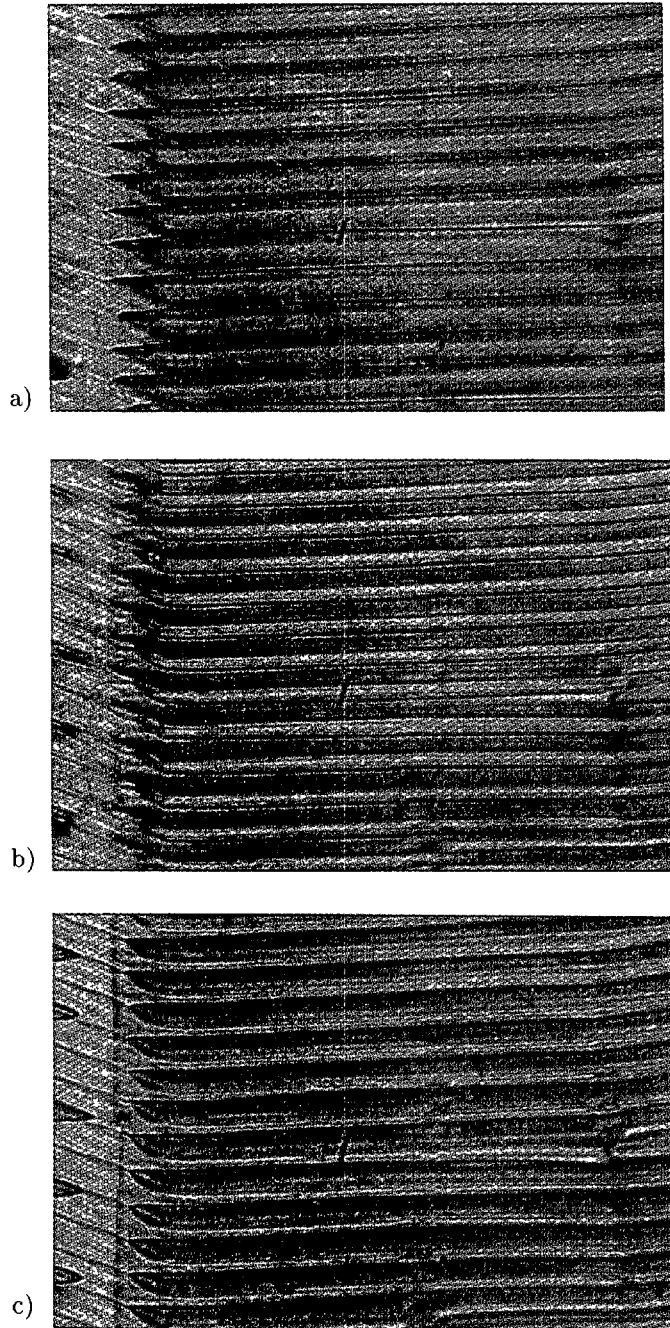


Photo 5. — Shifted lines when the cell thickness is more than twice the pitch: a) One family near the upper glass plate. b) Another family located on an intermediate level, the distance between the lines is divided in half. c) A third family, similar to the first one, near the lower glass plate. Same mixture as for the Photo 4 (p. 1715). Polarizers are in any position. Scale: 1 cm = 25 μm .

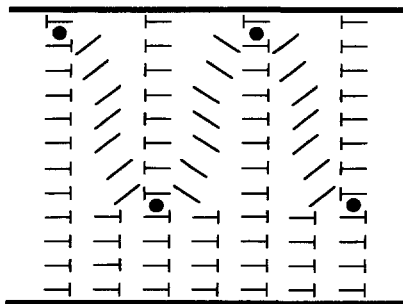


Fig. 25. — Director distribution in the case where the pair of lines does not occupy the whole thickness.

nature of this wall? To try to answer this question we have accurately observed a wedge shaped sample with a strong magnification. Photo 6 (p. 1723) shows that for thickness $d \simeq 3Z_0$, in the region located between the part where only one pair of shifted lines is observed and the part where two superposed pairs of lines are observed, one pair adds to the shifted pair in the empty space. What is the nature of this new pair?

Even observing very accurately the position of every line does not allow us to see if it is a shifted or a superposed pair. The only clear features of this texture are:

- in the intermediate level, the z distance between the lines is very constant and equal to $Z_0/2$;
- the background is almost black when the angle between the polarizer and the analyser is $\sim (\pi/2 \pm 2\theta)$, typical angle for a symmetrical anchoring.

Moreover, for this compound the position of the molecules is well defined on both plates treated with SiO ($-\theta$ on the upper plate, $+\theta$ on the lower one) that is for the polarization \mathbf{P} oriented toward the bulk. This is due to the interaction between \mathbf{P} and the polar surfaces [18.19].

3.1.3.2. Topological Interpretations. — Starting from this information we can try to give the distribution of the director in every case. The topology of the shifted lines given in the Section 1 is that of one pair of lines occupying the whole sample thickness.

- Figure 25 gives the topology when the pair of lines does not occupy the whole thickness. We include a wall close to the line far from the plate. Between this wall and the plate φ is constant, the director distribution is uniform.
- When a new pair adds we know that, in the intermediate level, the z distance is $Z_0/2$; it determines the position of the intermediate level line of the second pair.
- Figure 26 gives the topology if we suppose that the two lines of this second pair are shifted, with symmetrical anchoring. A rotation of $\varphi = \pi$ is to be added between the two pairs. What could justify such a rotation in so short a space?
- Figure 27 gives the topology if we suppose that the two lines of the second pair are superposed, with parallel anchoring. In this case at the wall level between the two pairs φ is constant. This topological interpretation is more convincing. In reference [16], Tsuchiya *et al.* were obliged to create several rotations to interpret the texture. In our

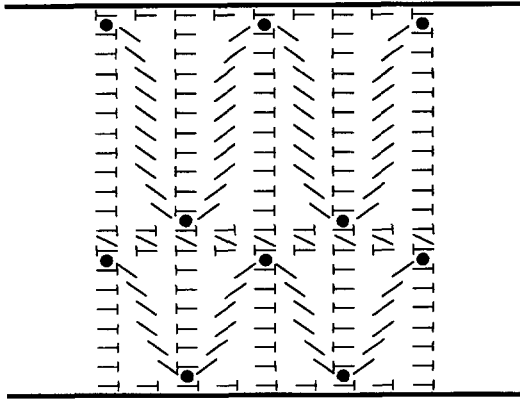


Fig. 26

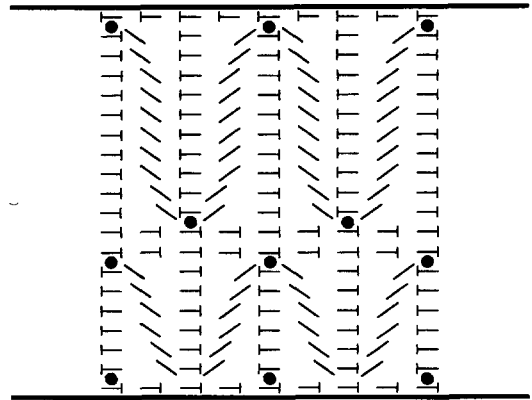


Fig. 27

Fig. 26. — Director distribution if both pairs of lines are shifted lines: a π rotation is necessary at the level situated between the pairs.

Fig. 27. — Director distribution if one pair of lines is a shifted one and the other pair a superposed one. This distribution does not imply a π rotation at the level situated between the pairs.

interpretation. the π rotation occurs in one of the two parts. The pair of shifted lines, connected to symmetrical anchoring, is more stable for small thickness than a pair of superposed lines which collapses easily in this case. When the thickness of the second part of the sample is large enough to allow a pair of superposed lines to be stable, the second helix forms and two kinds of pairs coexist. In this case, the distance between the other plate and the nearest line is also about $Z_0/8$.

At this point we can conclude that, from a topological point of view the best probability for the nature of the second pair is that of the superposed - with parallel anchoring - kind. But elastic considerations cannot give an account of this separation into two almost independent cells; there is between them a kind of grain boundary.

3.2. INTERPRETATION WITH THE HELP OF THE CHEVRON. — What is the nature of this wall dividing the sample into two parts? It seems as rigid as a plate since, while the theory gives the stable distance a equal to $Z_0/12$ in all cases, the lines can stay far from the plate, beyond this wall. It is obvious that these two parts in the same sample are equivalent to both sides of the chevron in thin cells: the “chevron texture” described by Rieker *et al.* [20] and Ouchi *et al.* [21] which explains typical defects called “zigzags”. We can at once suggest that, in spite of the “bookshelf geometry”, we get the “chevron” due to the shrinking of the smectic layers at the $S_A \rightarrow S_C^*$ transition.

The observations and the measurements previously explained prove that the chevron texture described for thin samples is also the texture of the thick samples. However, the plane of the chevron in thin cells is proposed [19] to be located closer to one plate than to the other. For thick samples several measurements, similar to that of paragraph 3.1.3.1, give no significant difference between the thickness values of the two parts.

We think that for thin cells the π rotation pushes away the wall and brings it closer to the plate situated near the uniform part. For thick cells this wall can be at equilibrium about in the middle between the two plates.

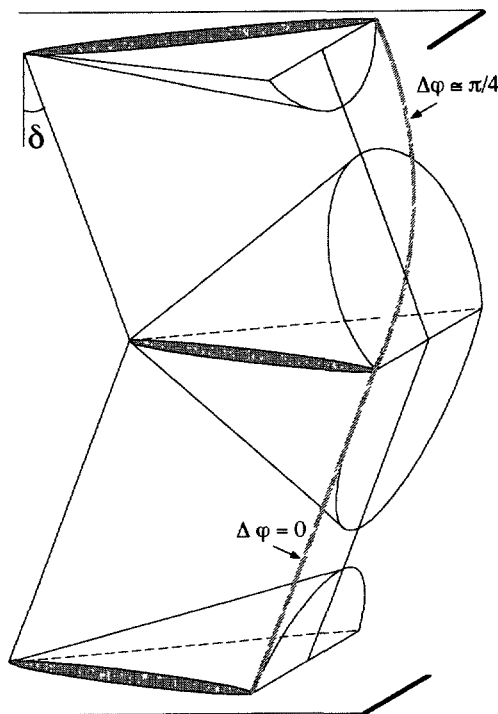


Fig. 28. — Intersection in the chevron plane of the cones belonging to the layers located on both sides of this plane. This intersection is due to the fact that the tilt of the layer δ is smaller than the cone angle θ . On one side of the chevron plane φ varies and on the other side it is constant.

3.2.1. Consequence of the Chevron Texture on the Line Positions. — We have now to see in more detail what is involved for the chevron for the situation of the defects and for the director field and whether it is in agreement with the theory. The model of the chevron given with many details by Clark *et al.* [22] based on X-rays experiments indicates a tilt of the layers $\delta < \theta_0$ and an orientation of the molecules along the intersection of the cones on the chevron plane (Fig. 28). If we continue to suppose no pretilt at all on the bounding surfaces, the anchoring directions are parallel to the intersections of the cones by these surfaces. On one side of the chevron plane, the director turns on the cone when one goes from the plate to the plane, but the variation of φ due to this rotation is different from π , the rotation angle for “bookshelf” geometry. On the other side of the chevron plane the director stays parallel to the plane of the second plate. With tilted layers the two senses of rotation of the director in the layer which connect symmetrical positions are not equivalent. Due to the tilt there is a component of the helix along x . Only one sense of the rotation on the cone gives the right sense of rotation for the helix for this component (Fig. 29). So the rotation is more probable with this sense.

3.2.1.1. Line Plate Distance. — In wedge shaped cells when the thickness increases the first pair of lines formed is located closer to one of the plates than to the other. This empty space cannot be explained by the theory of uniform layer structure. It is evident that this pair is situated on one side of the chevron plane, the empty part is on the other side. We saw in the Section 3.2.3.1 which the part of the chevron is occupied by this first pair of lines and we noted that the distance of one line to the plate for the mixture 50% DOBAMBC in its racemic is

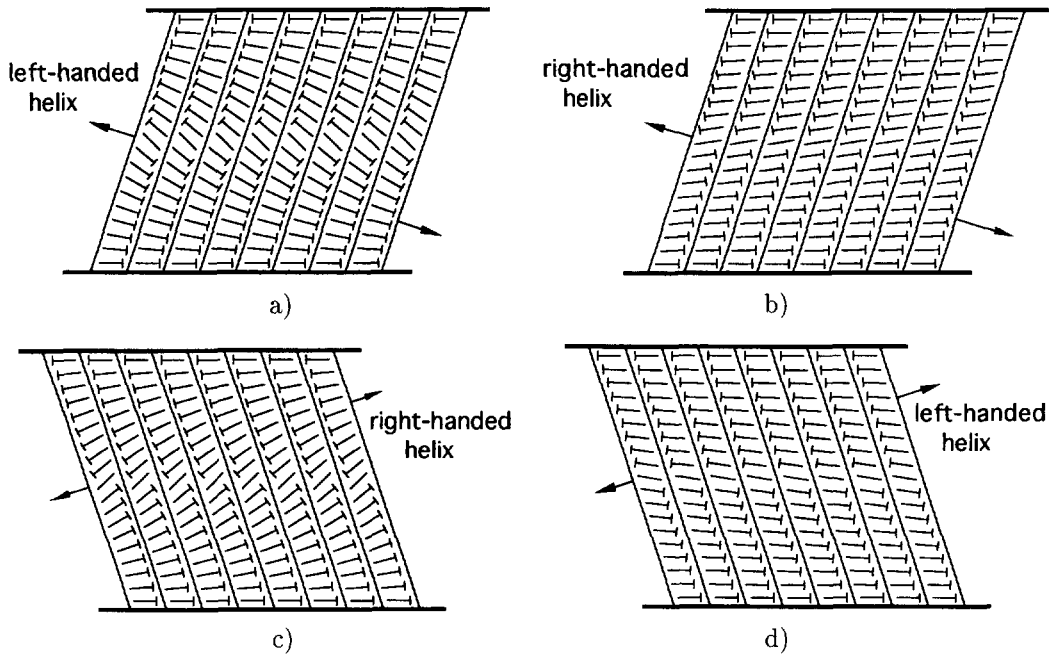


Fig. 29. — The anchoring directions are the same on each diagram: they are anti-parallel. a) The director rotates on the large part of the cone to go from the lower plate to the upper one. This rotation creates a left-handed helix whose axis is perpendicular to the smectic layers. b) With the same tilt of the layers, the director rotates on the small part of the cone. The helix is right-handed. c) The smectic layers tilt in the opposite direction. In this case when the director rotates on the large part of the cone the helix is right-handed. d) With the same tilt of the layers, when the director rotates on the small part of the cone the helix is left-handed. If the intrinsic helix of the compound is right-handed: e) On both parts of a zigzag wall, the helix due to the rotation has the correct sense but the director rotates on the large part of the cone. f) The helix also has the correct sense and the director rotates on the small part of the cone. This situation is the most probable. To choose this favorable distribution of the director the rotation takes place on the correct side of the chevron.

approximately $1 \mu\text{m}$. The thickness of the empty part is several microns. The theory accounts for the short distance, but not for the empty part, which can be explained by the chevron texture: each side of the plane is like a single cell and the distance of the second line to the chevron plane is of the order of the distance of the line to the plate: $1 \mu\text{m}$.

3.2.1.2. Relative Position. — We have described the relative position of the lines as superposed for parallel anchoring and with a half-pitch shift for symmetrical anchoring. But we supposed a “bookshelf” geometry, that is to say the smectic layers perpendicular to the plates. We have now to transform the topology described for a bookshelf geometry into a topology involving the chevron texture. We propose the field of the director in the thick chevron texture as in Figure 30. To build this topography we took as a basis that:

- the line is located in the smectic layer where on both sides of the disclination φ has changed by π ;
- the helix is right-handed;

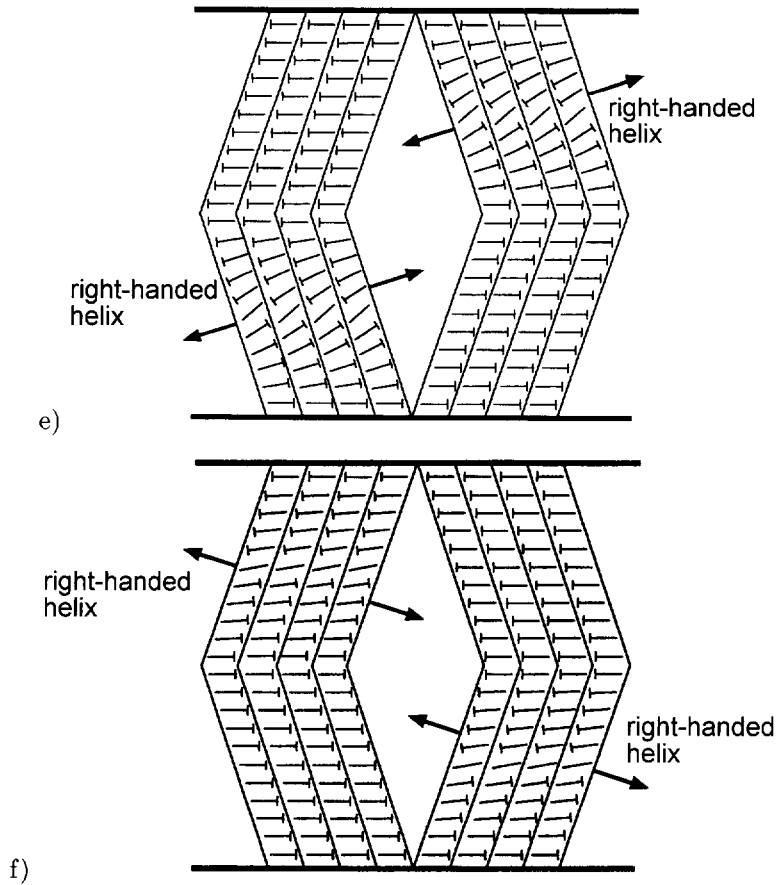


Fig. 29. — (Continued.)

- the apparent distance along z at the chevron level between one line on one side of the plane and the following line on the other side is half the pitch, what is deduced from accurate observations.

The first remark to be made about this topology is that the z distance between the two lines of a shifted pair is no longer $Z_0/2$ but alternately less and more than this value and that the two lines of a superposed pair are no longer one in front of the other.

3.2.2. Observed Line Positions. — What about the relative line positions observed in the cells?

The situation is more complicated in the case of symmetrical anchoring than in the case of parallel anchoring, because of the superposition of two pairs. However, some points are clear:

- In the part where there is only one pair of lines, that is where the thickness is not large enough to allow two helices, we have seen that the pitch can be larger than the spontaneous pitch. The distance along z between two lines located at the same level gives the value of the local pitch. Photo 5 (p. 1716) shows that the distance along z between two shifted lines of the same pair is smaller than half the local pitch. This difference is explained by the chevron texture as we can see in Figure 30.

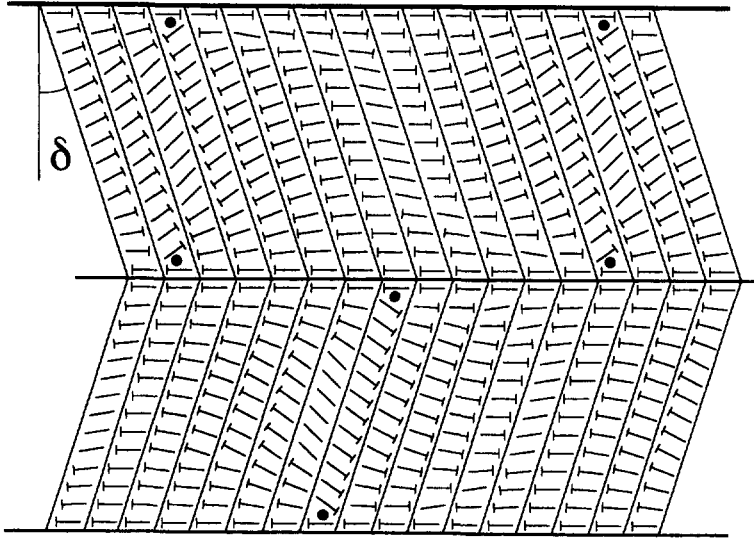


Fig. 30. — Distribution of the director with “shifted lines” on one side of the chevron plane and “superposed lines” on the other side. Due to the tilt of the layers and the planar anchoring of the molecules on the plates, the distance along x of two lines of the same “shifted” pair is no more $Z/2$, and the lines of the same “superposed” pair are shifted a lot, when they are observed from the direction of the normal to the glass plates.

- In the part where the second pair begins to form, while by topological considerations we have estimated that it is a superposed pair of lines, it is very difficult to see the position of the lines because there are four lines in the whole thickness (Photo 6, p. 1723).

Where the pairs are superposed, at the first and the third levels (Photos 5a-5b, p. 1716) the period of the lattice is the pitch Z_0 and at the second level (Photo 5c, p. 1716), the distance between two lines along z is $Z_0/2$. As it was indicated before, with a very large magnification two sub-levels can be observed where the distance between two lines is Z_0 . Here it is also very hard to note precisely the relative position of two lines of the same pair because four lines are located in the same place at several levels in the cell. Here the chevron also accounts for this situation.

We have to underline that the wall acts like a very rigid surface since the lines cannot cross it.

3.2.3. Some Comments. — Both pairs of lines now look like shifted lines. One of them is a shifted pair with symmetrical anchoring but the distance along z between two neighbouring lines is successively less and more than the half-pitch, as previously observed. The other pair is of a superposed kind, with parallel anchoring, but can seem shifted due to the tilt of the layers. However, with symmetrical anchoring we never observe superposed lines alone. We have seen in the Section 3.1.2 that these lines collapse more easily than shifted lines. That is why they appear when the thickness is larger, and the first lines to appear in the wedge-shaped cell are shifted lines.

In this interpretation we have considered the chevron plane as a rigid wall playing the same role as the glass plate. However, the fact that the distance along z between two lines on either side of the plane is the half-pitch suggests that there is an interaction between both

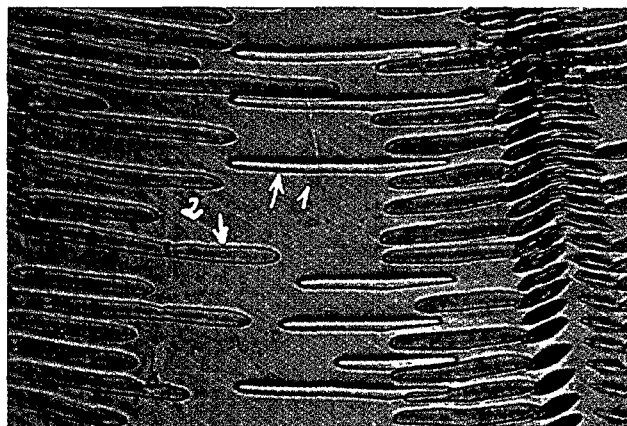


Photo 6

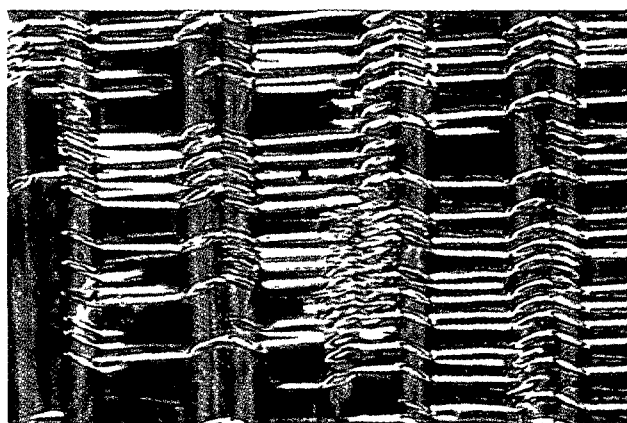


Photo 7

Photo 6. — Where the cell thickness is about twice the pitch, the first pairs (arrow n°1) adding to the shifted ones (arrow n°2) appear. They are not on the same level. Compound: a 50% mixture of chiral p-decyloxybenzylidene p'-amino 2-methyl butyl cinnamate (D.O.B.A.M.B.C.) with the racemic. Polarizers are in any position. Thickness: about 20 μm . Pitch: 10 μm .

Photo 7. — Even for thick cells, zigzags are observable (arrow n°1). The lines (arrow n°2) do not cross the zigzag defects which are decorated by small loops (arrow n°3). These loops occupy the whole thickness, because in the zigzags, the layers are in a bookshelf situation.

pairs through the chevron plane. The nature of this planar discontinuity is not completely understood.

To complete this interpretation we can give the slightly different topography in the case where, due to the interaction with the glass plates, as it has often been proposed, the molecules make an angle with them (Fig. 31). For the same tilt of the layers, the relative position of the lines is different.

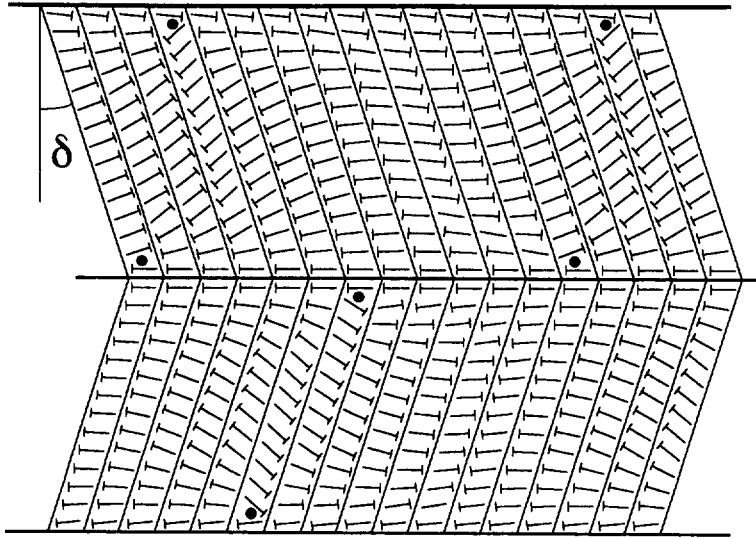


Fig. 31. — Distribution of the director if the molecules are no more planar but have a pretilt on the plates. The situation is slightly different from the previous figure. The lines of the “superposed” pair are not on the same layer and they also are shifted.

Another important observation is to be made: in thick cells there is the equivalent situation of the zigzag. When the two possible directions of the chevron meet, the zigzag wall is obvious. The lines do not cross the zigzag. The structure of this defect proposed by Clark shows clearly layers perpendicular to the plates. In Photo 7 (p. 1723) in this part we can see small loops decorating the wall. Their distance is the pitch. They exist where the thickness is too small to allow the other kinds of lines. This is a proof that this part of the zigzag wall is not divided by the chevron into two more narrow parts and this confirms the Clark’s structure of the zigzag defect.

All these observations confirm the structure of the cell given in the thin cell case and show that the structure is similar in the thick cell case; they are in good agreement with the theory.

Conclusion

The symmetry of the chiral smectic C structure induces complicated textures when the compound is confined between two glass plates treated to give definite anchoring. We have observed the thick sample textures to understand the orientation of the layers and the distribution of the director. The locations of the unwinding lines between the bounding surfaces have been evaluated: the distance between the glass and the line, the number of line-pairs in the whole thickness and the local distance between two pairs which gives the local pitch. The calculation of the involved energies in limited sample textures allows us to account for the experimental results for the line-plate distance, for the relative position of the two defect families and for the real pitch in the line texture. Furthermore, it gives the tilt angle variation around the defect, the smectic layer displacement variation, and the azimuthal angle variation. Everything has been calculated assuming the “bookshelf geometry”.

The presence of two pairs of lines between both glass plates implies another geometry for the smectic layers than that of the “bookshelf”. Starting from the “chevron” texture, proved

in thin samples, we can justify these two pairs in thick samples, which show that the chevron plane plays a role identical to a bounding surface: linear defects cannot cross this plane. In this plane the molecular orientation seems to be uniform. The sample looks like two individual samples upon over the other. Each one can be interpreted by the calculation made in the case of the simple "bookshelf" geometry.

References

- [1] Meyer R.B., Liébert L., Strzelecki L. and Keller P., *J. Phys. France Lett.* **36** (1975) 69.
- [2] Clark N.A. and Lagerwall S.T., *Appl. Phys. Lett.* **36** (1980) 899.
- [3] Handschy M.A., Clark N.A. and Lagerwall S.T., *Phys. Rev. Lett.* **51** (1983) 421.
- [4] Brunet M. and Williams C., *Ann. Phys.* **3** (1978) 237.
- [5] Glogarova M., Lejcek L., Pavel J., Janovec V. and Fousek J., *Mol. Cryst. Liq. Cryst.* **91** (1983) 309.
- [6] Monkade M., Boix M. and Durand G., *Europhy. Lett.* **5** (1988) 697.
- [7] Handschy M.A. and Clark N.A., *Ferroelectrics* **59** (1984) 69.
- [8] de Gennes P.G., *C. R. Acad. Sci. (Paris) B* **275** (1972) 939.
- [9] Frank F.C., *Disc. Faraday Soc.* **25** (1958) 19.
- [10] Galerne Y., Thèse, 15 février 1983, Orsay, France, p. 44.
- [11] de Gennes P.G., *Solid State Commun.* **10** (1972) 753.
- [12] Bartolino R. and Durand G., *Phys. Rev. Lett.* **39** (1977) 1346.
- [13] The calculation is made with a P.C. by the finite element method in a domain of size $Z/2 \times d/2$. In this domain we use 257×257 points. The derivatives on one point M are calculated with 2 points on both sides of M . The cubic equation is calculated by the Newton method. The starting values for the relaxation method are those calculated for the higher and the lower values of θ_0 . We stop the calculation when the difference between the results obtained with these two starting values are less than 1%. This kind of equations close to Laplace equations converge without problems in some hours.
- [14] Bourdon L., Sommeria J. and Kleman M., *J. Phys. France* **43** (1982) 77.
- [15] Glogarova M., Lejcek L., Pavel J., Janovec V. and Fousek J., *Czech. J. Phys. B* **32** (1982) 943.
- [16] Brunet M. and Isaert N., *Ferroelectrics* **84** (1988) 25.
- [17] Tsuchiya T., Ouchi Y., Ishikawa K., Takezoe H., Fukuda A., Kondo K., Era S. and Mukoh A., *Jpn J. Appl. Phys.* **24** (1985) Suppl. 24-2, 896.
- [18] Glogarova M. and Pavel J., *J. Phys. France* **45** (1984) 143.
- [19] Brunet M., Andersson G. and Lagerwall S.T., *Mol. Cryst. Liq. Cryst.* **152** (1987) 467.
- [20] Rieker T.P., Clark N.A., Smith G.S., Parmar D.S., Sirota E.B. and Safinya C.R., *Phys. Rev. Lett.* **59** (1987) 2658.
- [21] Ouchi Y., Lee J., Takezoe H., Fukuda A., Kondo K., Kitamura T. and Mukoh A., *Jpn J. Appl. Phys.* **27** (1988) L1993.
- [22] Clark N.A. and Rieker T.P., *Phy. Rev. A* **37** (1988) 1053.